DEVELOPMENT OF CELLULOSE ACETATE-BASED SCAFFOLD FOR BONE TISSUE ENGINEERING APPLICATIONS

BY

RUHIT SINHA

A thesis submitted in partial fulfillment of the requirements for the

Master of Science

Major in Mechanical Engineering

South Dakota State University

2020

THESIS ACCEPTANCE PAGE

Ruhit Sinha

This thesis is approved as a creditable and independent investigation by a candidate for the master's degree and is acceptable for meeting the thesis requirements for this degree. Acceptance of this does not imply that the conclusions reached by the candidate are necessarily the conclusions of the major department.

Anamika Prasad
Advisor Date

Kurt Bassett
Department Head Date

Dean, Graduate School Date

Dedicated to

all the scientists and doctors who are working to save lives

ACKNOWLEDGEMENTS

"Let us be a little humble; let us think that the truth may not perhaps be entirely with us."

- ***Pandit Jawaharlal Nehru***

I would like to convey my sincere gratitude to my thesis advisor Dr. Anamika Prasad for providing me constant support and direction to complete this work. She has a great contribution towards imbibing in me scientific temper and research ethics. I had a chance to attend one of her coursework: Advanced Stress Analysis in Mechanical Design (ME 741) that enabled to have depth and breadth of continuum mechanics. Her coursework: Mechanical Behavior of Biomaterials (ME592) installed a foundational knowledge about various biomaterials and bone tissue from biological and mechanical point of view, which helped to work on my thesis effectively.

I would like to thank my graduate thesis committee members: Dr. Srinivas Janaswamy and Dr. Zhong Hu who helped me with cellulose chemistry and computational solid mechanics with ANSYS APDL respectively. I would like to thank Dr. Travis Burgers and Dr. Saikat Basu who gave important suggestions during my graduate thesis seminar. I would like to thank Dr. Todd Letcher for training me the FTIR in METLAB. Trust me, it had a very significant role in this work. I would like to thank Dr. Kurt Bassett for offering Graduate Assistantship for two years work.

Finally, I would like to thank my parents: Mr. Rajmohan Sinha and Mrs. Gita Sinha, and my elder brother: Ranit Sinha for their emotional support being thousands of miles away. I had a great company with my lab-mates: Anirban Chakraborty, Mukesh Roy, and Trupti Mali and other graduate students: William Cahyadi, Amine Radoui, Christopher Santini, Shashikant Reddy and Sean Edeki.

TABLE OF CONTENTS

ABBREVIATIONS

Å	angstorm
nm	nanometer
μm	micrometer
cm	centimeter
g	gram
kg	kilogram
kN	kilonewton
Pa	pascal
kPa	kilopascal
MPa	megapascal
GPa	gigapascal
cm^3	cubic centimeter
m^3	cubic meter
με	microstrain
%	percentage
wt%	weight percent
rpm	revolutions per minute
°C	degree Celsius
mL	milliliter
Hz	hertz
s	second
min	minute

h	hour
mA	miliampere
kV	kilovolt
M_W	molecular weight
σ_T	mechanical strength
E	Elastic modulus / Young's modulus
ε_f	strain at fracture

LIST OF FIGURES:

LIST OF TABLES

ABSTRACT

DEVELOPMENT OF CELLULOSE-BASED SCAFFOLD FOR BONE TISSUE ENGINEERING APPLICATIONS

RUHIT SINHA

2020

Cellulose Acetate (CA) based biomaterials are being used as substrates for bone ingrowth applications due to their nontoxic and nonirritant nature coupled with optimum morphology and stiffness. Electrospinning with additives and/or post-treatment has emerged as a viable protocol to further improve mechanical properties of CA and expand its utility. Herein, we highlight the role of potassium chloride (KCl) in association with air-drying to enhance the elastic modulus and tensile strengths of CA fibers. Salt aggregation in between fibers is observed through Scanning Electron Microscopy (SEM), however, Fourier-transform infrared (FTIR) analysis signifies the interactions between K^+ ions and acetyl groups. The increase in KCl concentration (2 to 4 to 6%) boosts the elastic modulus to 176 MPa (52 times than pure CA) and tensile strength to 1.2 MPa (9 times than pure CA). The presence of K^+ ions, indeed, offers osteoconduction to fibers and thus the outcome has potential in bone tissue engineering applications.

Keywords: Electrospinning, Cellulose Acetate, Potassium Chloride, SEM, FT-IR, Bone Tissue Engineering

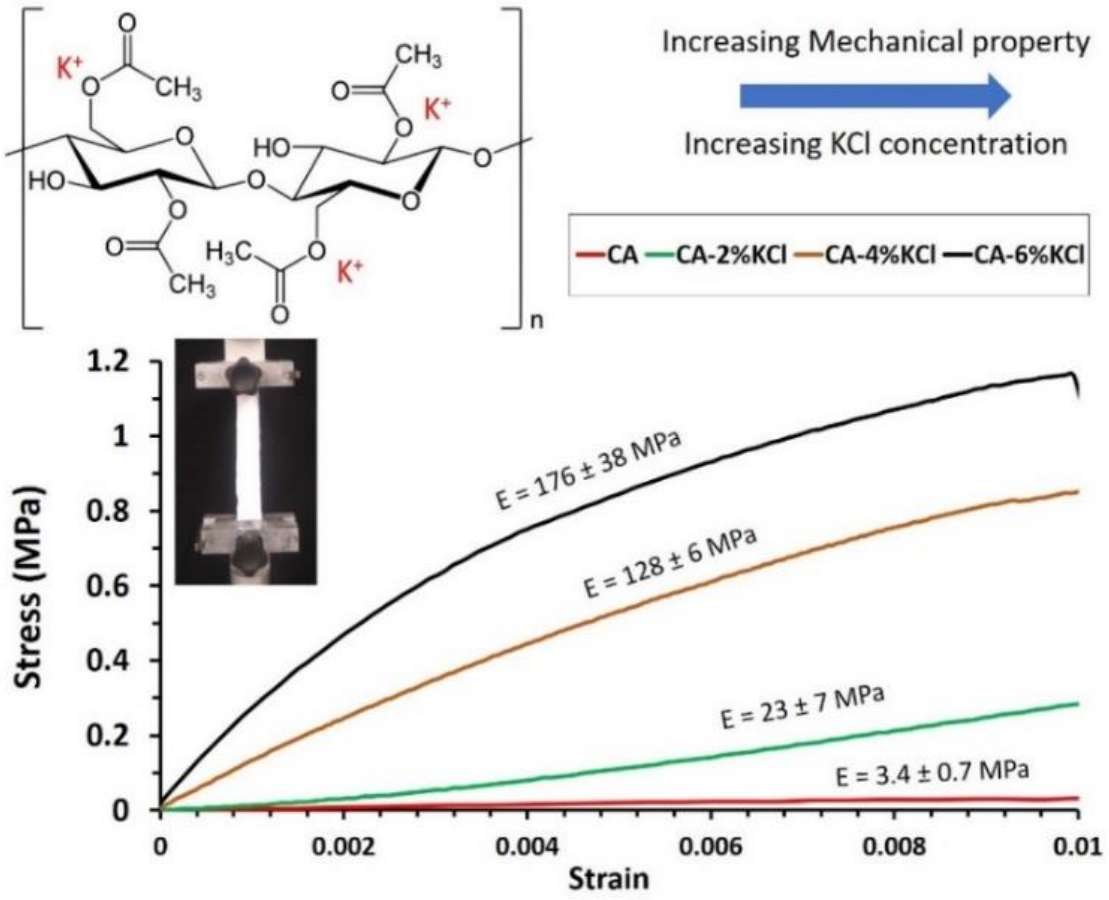

FIGURE 1: Summary of the work: Stiffness of CA-KCl fibers increases as the KCl concentration increases

CHAPTER 1: **INTRODUCTION**

Bone tumors both benign and malignant has peak incidence rate in adolescent and young adults and affects long bones of hand and legs. Reconstruction of these bones after tumor resection is a challenging problem including from the need to account for bone growth in younger patients. The use of bio-compatible scaffold with optimum compressive strength during recovery, together with osteogenic structure to support bone growth and regeneration is key in such applications. The use of most abundant organic polymer on earth: Cellulose, which is derived from non-animal sources, offers several advantages as bone scaffold (mechanical strength, fibrous structure similar to extra-cellular matrix, biocompatibility, and biodegradability) and can be a suitable biomaterial for bone tissue microenvironment as detailed in the following sections.

In this work, one of the widely used cellulose derivate- CA has been employed to make scaffold material. To enhance its mechanical property, electrospun CA fibers has been treated with KCl to form CA-KCl fibers. The elastic modulus of CA-KCl fibers has been modulated to 23, 128, and 176 MPa by treating with 2, 4 and 6 % KCl, respectively. Hence, the stiffness of the fibers can be tuned according to the mechanical property of the tissue required. As a comparison, the elastic modulus of trabecular bone been reported for a range of 10 to 20,000 MPa depending on porosity and density [1]–[5]

CHAPTER 2: **LITERATURE REVIEW**

2.1 BONE STRUCTURE AND PROPERTIES

Bone is a connective tissue that connects, supports, binds or separate other tissues or organs. From the materials point of view, Bone is a composite made up of different type of cells (osteoclast, osteoblast & osteocytes), organic substance such as water (10-20% of total weight), collagen(~28% of total weight) forming a matrix and inorganic substance such as tricalcium phosphate or hydroxyapatite (60-70% of its dry mass)[6], [7]. Type I collagen composes 95% of the organic matrix while the remaining 5% is proteoglycan, glycoproteins and other non-collagenous proteins [8]. The organic component is generally flexible and resilient while the inorganic component is hard and rigid. Bone are largely classified, based on the structure, into two types: Cortical and Cancellous (also called Trabecular) [6]. The former is compact, forms a dense cylinder down the shaft of a typical femur bone surrounding the central marrow cavity and has a much lower surface area due to lower porosity and constitutes 80% of the bone mass in human body [6]. While, the latter is spongy, highly porous, situated at the ends of the long bone and lesser Young's modulus. The gradual decrease in the modulus matches the properties of cortical bone to cartilage that forms the surface of femur head [6]. The most basic level of organization of bone is the nanostructured array of hydroxyapatite crystals embedded within collagen matrix. A mechanism of intrafibrillar mineralization of collagen has been hypothesized in which capillary action causes a fluidic amorphous precursor phase to induce highly anionic non-collagenous proteins of the bone matrix and to pull up into the zone holes and interstices

of collagen fibril that eventually solidifies as the hydration water excludes. The precursor finally crystallizes leaving behind nanocrystals of hydroxyapatite ($Ca_{10}(P0_4)_6(OH)_2$) embedded in collagen fibrils [7].

2.2 SCAFFOLD IN BONE TISSUE ENGINEERING APPLICATION

2.2.1 CERAMIC BASED SCAFFOLD

Bioglass 45S5 which is a bioactive glass ceramic material containing 45% SiO_2, 24.5% Na_2O, 24.5% CaO, and 6% P_2O_5 in weight percent have been showed to induce primary human osteoblasts in vitro [9]. The osteoblast proliferation evaluated after 2, 6, and 12 days was indicated by the flow cytometric analysis of cell cycle: the increase of cell population in both S and G2/M phases of cell cycle. Biochemical analysis of the osteoblast differentiation markers alkaline phosphatase (ALP) and osteocalcin further indicated augmentation of osteoblast commitment.

2.2.2 SYNTHETIC POLYMER BASED SCAFFOLD

Synthetic polymers on the other hand, are easily processed and tunable. These are, however, not bioactive and can cause inflammatory response. Therefore, biomolecules are attached to provide the required biological signals and to make it inert from immune responses. Some of the widely used polymer for the application are polyanhydride, polypropylene fumarate (PPF), polycaprolactone (PCL), polyphosphazene, polylactic acid (PLA), polyether ether ketone (PEEK) and poly(glycolic acid) (PGA) [10].

Poly (lactic-co-glycolic acid), shortly PLGA, in the composition of 75% lactic acid and 25% glycolic acid has been used for human osteoprogenitor cells in scaffolds with 200 μm mean pore size [11]. The polymer was then coupled with RGD peptides [using poly(L-lysine), or PLL] and physical adsorption of Fibronectin (FN). As stated earlier, the binding between integrin receptor and ligand is usually moderated through an Arg-Gly-Asp (RGD) recognition sequence. A variety of RGD-containing ligands, such as osteopontin, thrombospondin, and bone sialoprotein have been identified within bone that are important in cell motility, polarity, proliferation, and survival. There was significant enhancement in cell adhesion, spreading and differentiation with adsorption of FN and RGD peptides on the three-dimensional PLGA (75:25) scaffolds. This study signifies the potential of synthetic polymer scaffolds that mimic the extracellular matrix and support osteoblast-like cells adhesion and spreading.

2.2.3 NATURAL SCAFFOLD

Some of the natural polymers used for the application are collagen, fibrin, chitosan, hyaluronic acid, and alginate [12]. These are biocompatible and biologically active exhibiting osteoconductivity and low immunogenicity. However, it has limitations of possessing low mechanical properties, higher degradation rate and chemical modification for tissue engineering [13].

Silk fibroin, an insoluble fibrous protein produced by the silkworm, Bombyx mori, have also been explored for human osteoblast-like Saos-2 cell and fibroblast cell support matrixes [14], and engineering bone tissue in vitro using human derived mesenchymal stem cells [15]. The silk fibers had a significant variation in diameter as a result of which the

elastic modulus was found to vary from 8.9 GPa to 17.4 GPa while yield stress from 126 MPa to 231 MPa. Interestingly, unloading/reloading tests demonstrated that the stress-strain relationship isn't sensitive to strain rate [16]. Microstructurally, mechanisms such as breakup of crystalline regions that decrease tensile strength must have balanced the deformation mechanisms such as increased alignment of chains that increase tensile modulus. In another study, porous 3D scaffolds of silk were produced using freeze-drying, salt leaching and gas foaming techniques. The latter two used porogens NaCl and NH_4HCO_3 respectively that produced a combination of high compressive strength, interconnected pores, and pore sizes greater than 100 μm. The maximum compressive strength was calculated to be 30 ± 2 kPa, 175 ± 3 kPa, and 280 ± 4 kPa respectively while the porosity was around 99%, 84-98% and 87-97% respectively [17].

2.3 CELLULOSE

2.3.1 SOURCE

Cellulose is a polysaccharide consisting of D-glucose units connected by a glycosidic bond between OH group of C4 and C1 carbon atom [13]. The term was first used in 1839 by a French chemist Anselme Payen who determined its molecular formula $C_6H_{10}O_5$ using elemental analysis. The chain length of the polymer is expressed in degree of polymerization (DP), i.e. number of monomer units or repeat units in cases where repeat unit may not be identical to monomer unit, that varies from origin and treatment of raw material. Cellulose is the most abundant polymer on earth produced by plants, fungi, algae, and bacteria [14].

The bacterial cellulose (BC) was first discovered by a British scientist AJ Brown in 1886 on culturing Acetobacter under static condition [14]. Nowadays, BC is produced from wide range of bacteria such as Agrobacterium, Pseudomonas, Rhizobium, and Escherichia among which Acetobacter xylinus is considered to have the strongest ability of cellulose synthesis [14]. During the synthesis, the glucose chain that had been produced inside the cell thrust out via pores in the envelope, that combine to form microfibrils and eventually cellulose nanofibers [15]. Usually, there are two different methods of synthesizing BC: static culture and agitated culture. In static culture, the BC is produced at the air-liquid interface in thin membrane form whose thickness increases with longer cultivation time till oxygen is deficient causing the cells to die. In agitated culture, cellulose is dispersedly produced in round form faster than the former but with inferior crystallinity, degree of polymerization and strength [15],[8].

2.3.2 STRUCTURE

Morphologically, cellulose structure is similar to the collagenous structure of bone. The molecular structure of cellulose is responsible for several of its characteristics such as chirality, hydrophilicity, slow degradability, low cytotoxicity and a wide chemical variability due to the high donor reactivity of the OH groups [18], [19]. To further improve the ability of repairing bone damage, some bone components such as hydroxyapatite, growth factors and extracellular matrix protein, bone marrow mesenchymal stem cells, and estrogen are often injected into the cellulose structure [19], [20].

For instance, treatment of cellulose films adsorbing carboxymethyl cellulose activates nucleation of calcium deficient hydroxyapatite added that increases cell adhesion and

induces the differentiation of progenitor cell [19]. It has been shown that BC has a good biocompatibility and induced differentiation of mouse fibroblast-like C2C12 cells into osteoblasts in the presence of bone morphogenetic protein-2 (BMP-2) in vitro, as demonstrated by alkaline phosphatase activity assay. Calcium deposition and in vivo bone growth was increased with BMP-2 loading [21]. The study suggested BC to be good locally delivery system for BMPs and a potential scaffold material in tissue engineering. In another study, the effect of thickness of resorbable cellulose membrane on guided bone regeneration was investigated. It was found that out of 0.10 mm, 0.15 mm and 0.20 mm thick barrier membranes, 0.10 mm induced the most effective bone regeneration [22].

In another study, horse-derived mesenchymal stem cells were injected into bacterial cellulose scaffold whose pore provided support for differentiation into chondrocytes and bone cells. Bone marrow stem cells secrete cytokines and play a major role in regulation of osteoclast differentiation, mobilizing and proliferation of osteoblasts and angiogenic cells [19]. Noh et al. incorporated human umbilical cord mesenchymal stem cells (UCB-MSC) on BC-collagen scaffold for culture and found that the stability of the scaffold and calcium deposition is increased when the BC content is increased, indicating that the scaffold with higher BC content supports late differentiation. It was estimated that BC-Collagen in the ratio 5:1 was able to maintain a stable porous structure enabling nutrient access and oxygen for better diffusion. Subcutaneous transplantation experiments on the UCB-MSC loaded BC-Collagen scaffold showed more red blood cells and α-SMA (angiogenic markers) indicating neovascularization which is very crucial for providing nutrients during early stage of bone regeneration [23].

Estrogen has also significant role in bone formation and resorption by osteoblasts and osteoclasts respectively. Phytoestrogens has been reported to regulate the balance between osteogenesis and adipogenesis differentiation of mesenchymal stem cells [19].

While BC is pure cellulose, plant-based cellulose contains impurities such as hemicellulose, lignin, and possess higher constituent of cellulose Iβ and less crystallinity [24]. The microfibrils of plant cellulose are usually larger than those of BC and hence, is usually adjusted by changing the culture condition and the source organism.

2.3.3 MECHANICAL PROPERTIES: COMPARISON WITH BONE

The complexity and properties of bone such as porosity, pore size, mechanical properties, mineral density, cell type and cytokine gradients depends on a number of factors such as age, gender, nutrition, mechanical loading experienced in various activities, and disease state of the individual [25]. For instance, the elastic modulus of bone increases to a certain age and then decreases at 2% per decade; 3, 5, 35 year old human femur specimen had values 7.0, 12.8, 16.7 GPa respectively [25], [26]. The average trabecular Young's modulus measured using ultrasonic and micro-tensile testing was 14.8 ± 1.4 GPa and 10.4 ± 3.5 GPa respectively and the average Young's modulus of micro specimens of cortical bone measured using ultrasonic and micro-tensile testing was 20.7 ± 1.9 GPa and 18.6 ± 3.5 GPa respectively [27]. It is to be noted that the specimens were dried before micro-tensile testing so Young's Modulus values may have been greater than those of trabecular bone in vivo.

Another important factor is porosity which is also related to apparent density. Porosity is defined as percentage of void space in a solid [25]. Pores are crucial for bone tissue

formation as they facilitate migration and proliferation of osteoblast and mesenchymal cells, along with vascularization [25]. Unlike cortical bone, cancellous bone is highly porous and has a large surface area. It is 50-90% porous and pore sizes in the order of 1mm in diameter [25]. It is about 25–30% as dense, 5–10% as stiff, and five times as ductile as cortical bone. The energy absorption capacity of cancellous bone is considerably higher under compressive loads than under tensile loads. There are several studies for correlating Elastic Modulus of bone with porosity [27]. For any biomaterial scaffold, pore size of more than 300μm is recommended owing to enhanced new bone and capillary formation. Pore size has been shown to have significant affect in the osteogenesis due to vascularization. Small pores promoted hypoxic condition inducing osteochondral formation involving cartilage and bone cells. On the other hand, after vascularization, large pores lead to osteogenesis i.e. formation of bone without preceding cartilage formation [25].

Cellulose has been reported to have a wide range of mechanical properties and porosities. In a theoretical study based on lattice dynamical treatment considering the crystal structure to be monoclinic, the calculated Young's modulus along chain axis for native and regenerated cellulose was 167.5 GPa and 162.1 GPa respectively [28]. The Young's modulus was found affected by intramolecular hydrogen bond the especially the bond between the ether oxygen atom of the glucose ring and the hydroxyl side group, rather than the intermolecular hydrogen bonds. A calculation neglecting this hydrogen bond reduces the modulus by 40 % [28]. In one experiment, however, the Young's modulus of bacterial cellulose has been shown to be as high as 16.9 GPa in any direction across the plane of sheet and the tensile strength to be 256 MPa at an elongation of 1.7 % [29]. Likewise, artificially obtained cellulose using wet spinning of wood and tunicate cellulose nanofibers

had a Young's modulus of 23.6 GPa, tensile strength of 321 MPa, and elongation at break of 2.2%. The methods of drying the cellulose samples prepared can also affect the mechanical properties. For instance, gelatinous bacterial cellulose when dried by lyophilizer and oven had a Young's modulus of 6.65 MPa and 18.12 MPa respectively, and Tensile Strength of 11.94 MPa and and 328.79 MPa [30].

Nonetheless, the mechanical properties of cellulose can be enhanced by adding other materials. One such example is carbon nanotubes dispersed in electrospun cellulose acetate fibers forming a composite that increased the tensile strength and Young's Modulus by about 64% and 80% respectively compared to pure cellulose acetate nanofibers [31]. In another example, addition of graphene oxide to electrospun cellulose acetate increased the tensile strength and Young's modulus of the composite nanofibers by about 73% and 75%, respectively, compared to those of pure cellulose acetate nanofibers [32].

The fact that intramolecular hydrogen bonds are responsible for the strength of cellulose can be exploited to enhance the mechanical property. In a study, the tensile strength of Zn-cellulose film with value 21.7 kPa was increased by 250% with addition of Ca^{2+} ions (Ca:Zn = 0.03 Molar ratio) . Further addition of Ca^{2+} ions (Ca:Zn = 0.06 Molar ratio) augmented to 350% rise. The possible mechanism for the change is attributed to formation of nanofibrils due to the creation of intermolecular bonds between subsequently added Ca^{2+} ions and the free Zn-cellulose chains through cooperative interactions between the hydroxyl groups, Zn^{2+} ions and water molecules.[33]

Cellulose acetate represents an interesting material, since it is biodegradable and exhibits mineralization, a property that is crucial to an efficient disposal, namely by composting treatment. This method is among the emerging technologies that may contribute to a better

solid waste management. Moreover, is it advantageous over other classical polymers used as matrixes, such as poly(vinyl alcohol) (PVA), which is biodegradable in solution but undergoes a very limited mineralization in solid mixtures [34].

2.4 CELL ADHESION

Integrins are heterodimeric proteins with two membrane-spanning subunits that bind to the extracellular matrix (ECM) proteins clustering together to form assembly of focal adhesions at which cell attaches with ECM [35]. Many of these adhesive proteins present in the extracellular matrix contain tripeptide arginine-glycine-aspartic acid (RGD) as their cell recognition cite [36]. These proteins include fibronectin, vitronectin, osteopontin, collagens, thrombospondin, fibrinogen and von Wille-brand factor. Other non-RGD-containing binding domains exist such as such as tyrosine-isoleucine-gly- cine-serine-arginine (-YIGSR-) and isoleucine-lysine- valine-alanine-valine- (IKVAV) in laminin [37], arginine- glutamate-aspartate-arginine-valine (-REDRV-) and -leucine-aspartic acid-valine (LDV) in fibronectin[38], -aspartate-glycine-glutamate-alanine- (DGEA) in collagen I, and various heparin-binding domains [39].

In another study, the peptide sequences -Arg-Gly-Asp- (-RGD-) and -Phe-His-Arg-Arg-Ile-Lys-Ala- (-FHRRIKA-) or mixtures of the two in the ratios of 75:25 (mimetic peptide surface I), 25:75 (mimetic peptide surface II), and 50:50 (mimetic peptide surface III) were immobilized on model surfaces using a heterobifunctional cross-linker to link the peptide(s) to amine- functionalized quartz surfaces. Mimetic peptide surface II (MPS II) and MPS III supported the highest degree of cell spreading ($p < 0.05$), following 4 h of

incubation, compared to MPS I, homogeneous -RGD-, and homogeneous -FHR- RIKA-grafted surfaces [38].

Regarding cellulose, the peptide chain Ile-Lys-Val-Ala-Val (IKVAV) was fused to a carbohydrate-binding module (CBM3) and modified the cellulose surface. The effect of these recombinant proteins IKVAV-CBM3 and (19) IKVAV-CBM3 as well as RGD-CBM3 was evaluated by MTS colorimetric assay and found that (19)IKVAV-CBM3 improved the adhesion of neuronal and mesenchymal cells with other cell lineages being unaffected [40].

2.5 DEGRADATION

Although it is very important that the scaffold morphology and mechanical property should support cell proliferation, it is equally important for the scaffold to degrade and eventually replaced by ECM in sync with the tissue regeneration.

One such degradation study was carried out on cellulose acetate scaffolds loaded with dexamethasone in order to evaluate the mass loss of polymer and the changes in the macrostructure [41]. The molecular weight of the polymer influenced the degradation rate and the higher the molecular weight is, the lower the degradation rate becomes, because there is a greater number of ester bonds to be cleaved due to the bigger chain length.

In another study, the primary mechanism of degradation of nano-bacterial cellulose was identified to be the disconnection of partial C-O-C bonds under the action of water molecules and ions when immersed in Phosphate Buffer Solution. The degradation ratio defined as the percentage of reducing sugar to the original weight increased from 5% in first week to 9.8% in thirty third week [42].

2.6 RESEARCH OBJECTIVE

Our objective is to take care not only the mechanical property of bone tissue but also to consider the nature of cell adhesion, degradation and morphology while developing a biomaterial for bone tissue engineering application. The mechanical property of our proposed material CA needs to be enhanced to be comparable to bone. The following chapter will discuss in detail one such strategy where potassium chloride has been used to enhance the mechanical properties of CA.

CHAPTER 3: ENHANCING MECHANICAL PROPERTIES OF ELECTROSPUN CELLULOSE ACETATE FIBERS UPON POTASSIUM CHLORIDE EXPOSURE

3.1 INTRODUCTION

Cellulose is the most abundant organic compound found on earth. Due to favorable mechanical properties, biocompatibility and degradability, one of its derivatives: Cellulose acetate (CA) based scaffolds are being used in widespread biomedical applications such as for bone [43]–[45], cartilage[46], skin[47], and neural tissue regeneration[48], among others. In these applications fibrous scaffold structure similar to the extracellular matrix that can support cell function and growth for tissue regeneration is critical. Toward this end, electrospinning has emerged as a viable, cost-effective and successful tool to engineer submicron to nanoscale fibers [49].

The morphology of the electrospun fibers can be fine-tuned to meet the specific application requirements by controlling the electrospinning parameters namely voltage, types of collectors, and solvent(s), the concentration of the solution, flow rate and tip-to-collector distance [50]. In this parameter set, solvent plays a critical role in producing uniform, ultrafine and defect-free fibers. Importantly, solvents with lower surface tension, e.g., acetone, with highest dispersion force [51] are favored in forming finer electrospun fibers

are favored. For example, bead-free CA fibers with 1 μm diameter could be produced with acetone as the solvent [52]

Electrospun CA fibers with elastic modulus varying from 1 MPa to 400 MPa, tensile strength from 1.2 MPa to 49 MPa [31], [53]–[57] and fiber diameter from 35 nm to 65,000 nm[51] have been reported. The observed variations are due to differences in processing environment (temperature and pressure), electrospinning parameters, and strain rates (Table 2). Tests conducted at a higher strain rate exhibit enhanced stiffness and strength than those performed at lower strain rates [58]. Overall, pure CA fibers are fluffy and have inadequate mechanical strengths for most applications. Thus, modifications are warranted to enhance mechanical properties, e.g., through additives and/or post-treatment.

Several studies have evaluated such modifications for CA-based fiber formation. For instance, heat treatment at 208 °C for 1h augments tensile strength to 5 MPa from the initial 1.2 MPa [53]. Fusion of fibers just above the glass-transition temperature appears to be responsible for the observed increase. Similarly, deacetylation with Na_2CO_3 followed by washing resulted in 2.5 times increase in tensile strength from 2.16 to 5.24 MPa due to its conversion to pure cellulose, enabling newly formed hydroxyl groups holding the chains tighter via hydrogen bonds [54]. Modifications involving certain additives and fillers led to even more remarkable changes in the mechanical properties. For example, presence of 0.5 wt% carbon nanotube elevates the tensile strength by about 3 times: 40 to 135 MPa and Young's modulus by about 11 times: 100 to 1100 MPa [31]. Similarly, graphene and graphene-COOH upsurge the Young's modulus to 910 MPa from the initial 245 MPa (pure CA)[55]. In another study, the CA-Graphene oxide composite demonstrated tensile

strength from 400 MPa to 1600 MPa and Young's modulus from 49 MPa to 97.5 MPa compared to pure CA values [56].

Another approach of strengthening CA material is by use of natural fillers such as collagen and chitosan. The CA matrix impregnation with these biopolymers, as fillers to form sponge-woven scaffolds, results with a tensile strength of 40 MPa and Young's modulus of 600 MPa compared to pure CA with values 3.8 MPa and 34.7 MPa respectively [57]. In another study, Chitosan/cellulose acetate nanofibers fabricated through electrospinning demonstrated higher tensile strength of 17 MPa compared to 2.2 MPa of pure CA [54].

The examples stated above suggest the seminal role of additives on improving the mechanical properties of CA fibers. The choice of additives or post-processing also depends on targeted applications. Additives that potentially show bioactivity to enhance tissue regeneration and osteointegration will be preferred for applications such as bone tissue. It has been demonstrated in an ex-vivo cell-culture experiment that potassium ions release from the alkaline treated calcium phosphate coating of Ti-24Nb-4ZR-7.6Sn alloy can promote osteoblast adhesion and proliferation [59]. A similar in-vitro study of human alveolar bone cell culture on ion-implanted titanium found the influence of $^{40}Ca^{+}$ and $^{39}K^{+}$ ions on the surface chemistry enhancing the osseointegration [60]. In the context of cellulose, inorganic non-aggressive solvents including potassium chloride (KCl) solution (in water) has been used for cellulose solubilization and mechanical property modulation by chemically interacting with cellulose polymer backbone [33].

Hence, the above leads us to hypothesize that KCl solution can be used to modulate the mechanical properties of electrospun CA fibers, which can have potential promising

applications for bone tissue engineering. Towards the end, here we investigate the interactions and strengthening influences of K^+ ions on electrospun CA fibers by treating with varying concentrations of KCl (CA-KCl fibers). The structure and response of native and processed CA-KCl fibers are analyzed using a multiple of experimental techniques to identify the underlying mechanisms.

3.2 MATERIALS AND METHODS

3.2.1 MATERIALS

Cellulose Acetate with average molecular weight 30,000 g/mol and degree of acetylation 39.8% was purchased from Sigma Aldrich. Acetone of HPLC Grade was purchased from EMD Millipore. Potassium Chloride (KCl) was purchased from VWR. All the chemicals were used as received without further purification.

3.2.2 ELECTROSPINNING

Cellulose-based fibers were prepared using an in-house built electrospinning platform consisting of a 20 mL syringe with a 14-gauge spinneret and Chemyx Fusion 100 pump, a rack Mounting Linear regulated power supply (Acopian), and arrangement with static and roller collector. FIGURE 2 shows the setup with the components marked.

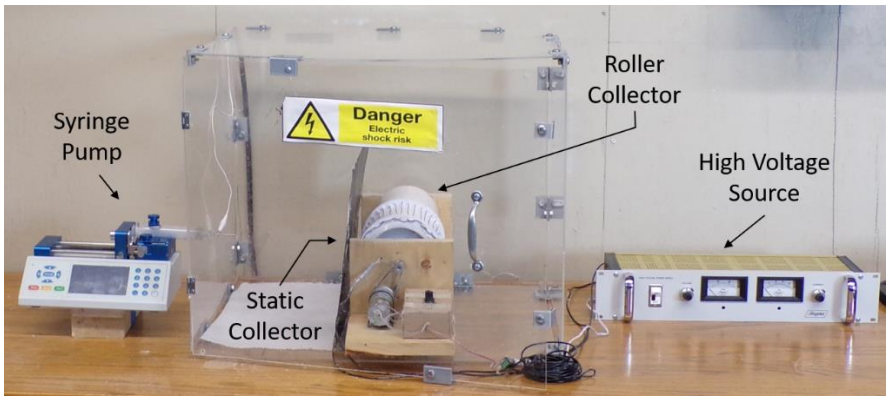

FIGURE 2: The In-house electrospinning setup used in the study with its major components marked

A solution of 15 wt% cellulose acetate was dissolved in acetone using hot plate and magnetic stirrer at 150 rpm and 22 °C for around 20 minutes until a homogenous solution was achieved. Since higher concentration contributed to increased viscosity [51][52], a 15 wt% solution was viscous enough to form bead-free fibers. The electrospinning parameters included a flow rate of 0.2 mL/min, an applied voltage of 15 kV, and a static horizontal collector made of aluminum foil with dimension 35 cm x 15 cm at around 18 cm from the spinneret. The electrospinning was performed for approximately 125 min at room temperature and normal humidity. The volatile nature of acetone enabled easy peeling of the fiber mat from the foil. However, the spinneret needs to be cleaned regularly due to clogging to maintain the uniformity of fiber generation.

*Please refer to the original source for this section: R. Sinha, S. Janaswamy, and A. Prasad, "Enhancing mechanical properties of Electrospun Cellulose Acetate Fiber Mat upon Potassium Chloride exposure," *Materialia*, vol.14, December 2020, Article 100881* 19

3.2.3 SAMPLE PREPARATION

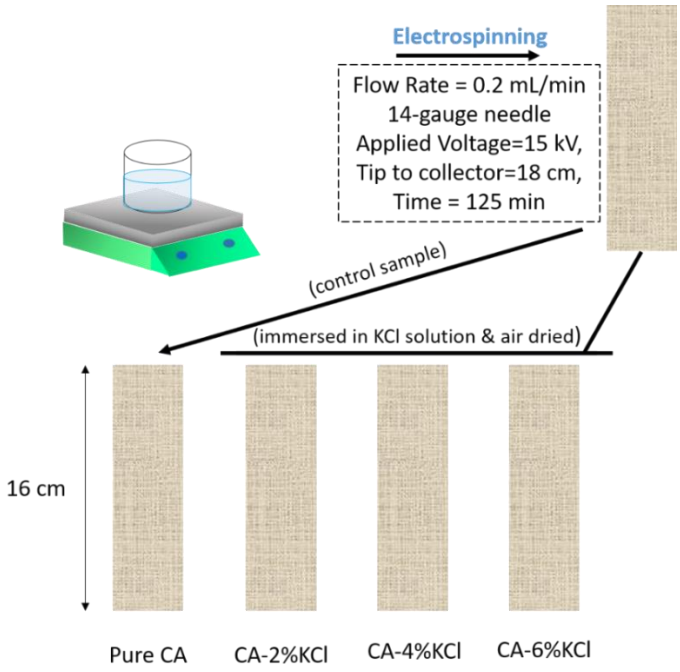

FIGURE 3: Preparation of samples

The fibers formed on the collector were peeled off gently, folded three times and kept under a weight overnight to flatten. The thickness of the folded mat was found to be around 3 mm. The middle portion with dimension 16 x 2 cm was cut out to form a testing sample as shown in FIGURE 4a.

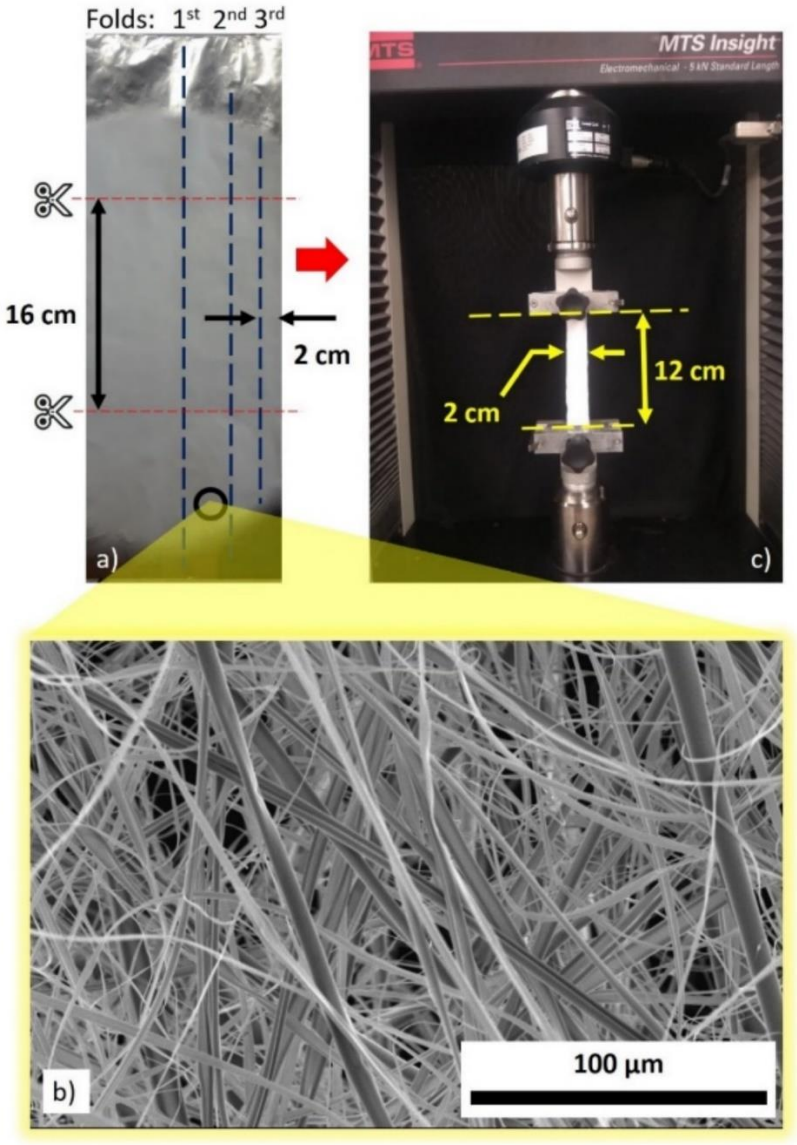

FIGURE 4: a) Folding of the fiber mat to form a testing sample of size 16 cm x 2cm; b) Scanning electron microscopy image of pure CA; c) Tensile test setup with fabric clamp and gauge length of the sample = 12 cm

A set of ten samples were tested as such with no post treatment. Other samples were post treated by dipping in potassium chloride (KCl) solution of varying concentration (2%, 4% and 6%) and air dried overnight at room temperature. The dipping and post drying resulted

in shrinkage of the mat to a thickness of approximately 2 mm. Post treatment with KCl was repeated with two other batch drying inside incubators at temperatures: 37 °C (Panasonic CellIQ CO2 Incubator) and 65 °C (Blue M 100A Dry Type Bacteriological).

3.2.4 CHARACTERIZATION

The weight of the post processed fibers was measured and a relative total weight for each set of fiber was reported. Several tests were carried out for fiber characterization and mechanical strength evaluation as indicated in FIGURE 4 b and c respectively. Tensile test was used for mechanical strength and scanning electron microscopy (SEM) was used for fiber morphology of electrospun mat.

3.2.4.1 SCANNING ELECTRON MICROSCOPY

Scanning Electron Microscopy was performed using Hitachi S-3400N**.** Prior to the observation, a piece of 5mm x 5mm fiber mat was cut out with scissors and placed in the specimen holder. They were sputter-coated using a CRC sputtering device with gold to minimize the electrostatic charge build-up on the nonconductive surface. The Au layer was 10 nm thick layer suitable for improving the quality of the high-resolution secondary-electron signal and prevent thermal damage [61]. The deposition was done at the rate of 0.2 $Å s^{-1}$ and the current setting of 35 mA on a 2-inch diameter, 0.125-inch thick target from Kurt J Lesker Co. (www.lesker.com). The surfaces were observed at 10 kV.

3.2.4.2 UNIAXIAL TENSILE TEST

The uniaxial tensile test was performed using Insight 4 (MTS Electromechanical Testing Systems) equipped with a 5 kN load cell. These tests were carried at a strain rate of 2 mm/min with a data acquisition rate of 50 Hz. The load versus deformation data was

obtained directly without using externally strain gauge or digital image-correlation method. Mechanical properties such as elastic modulus, tensile strength, and percentage strain at failure were determined and reported. Further, mean and standard deviation values were calculated, and significant differences using the t-test were established wherever necessary.

3.2.4.3 FOURIER-TRANSFORM INFRARED RADIATION

In addition, to understand the nature of interaction between potassium chloride and cellulose acetate fibers, a Fourier transform analysis was performed using Perkin Elmer Spectrum 65 FT-TR Spectrometer.

3.3 RESULTS AND DISCUSSIONS

3.3.1 RELATIVE WEIGHT AND FIBER MORPHOLOGY

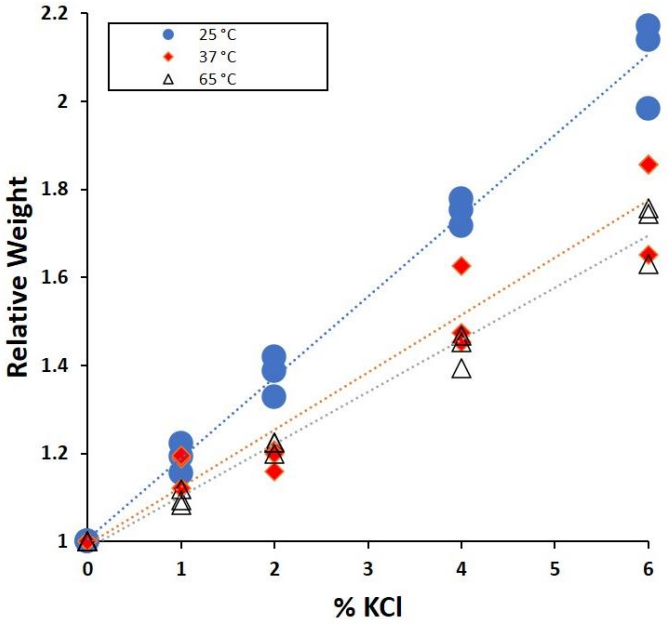

FIGURE 5: Relative total weight in post-processed CA fibers air-dried at room temperature, 37 °C and 65 °C. Number of samples = 3 for each set of fibers (1%, 2%, 4% and 6% KCl)

The relative weight of the CA-KCl fibers was measured and reported in FIGURE 5. It was observed that the relative weight increased as the concentration of KCl increased for all three drying temperatures, indicating a rise of salt deposition on the surfaces of fibers. The slope becomes smaller with an increase in drying temperatures to 37 °C and 65 °C. This potentially indicates higher total evaporation of moisture trapped within the fibers at higher temperature.

A closer look at the morphology of CA-KCl fibers using SEM revealed clusters of salt deposits randomly on the fiber mat, physically bridging the intersecting fibers (FIGURE 6). The salt deposition increased with the KCl concentration. Also, fewer clusters were observed at higher drying temperatures, probably due to greater dispersion of KCl solution.

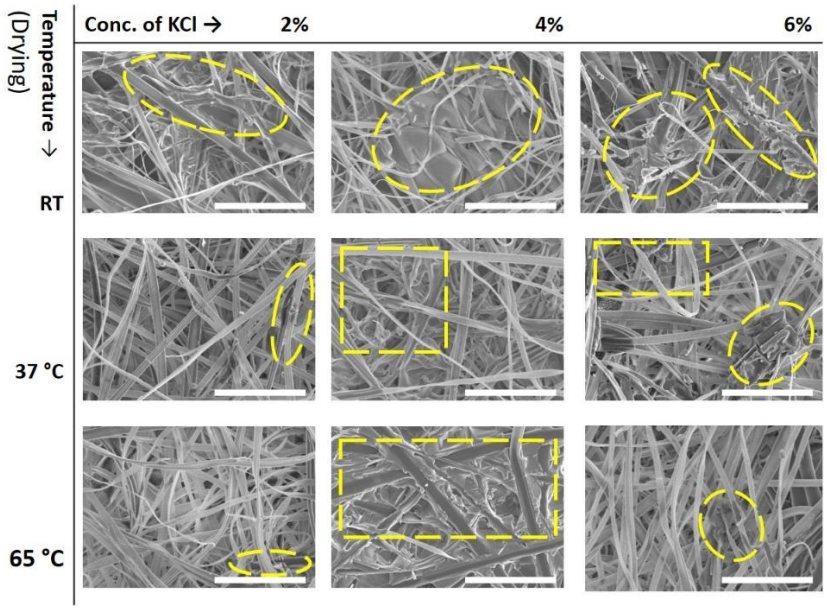

FIGURE 6: Matrix of SEM images of CA-KCl fibers with the concentration of KCl increasing (2%, 4%, and 6%) from left to right, and drying temperature rising (RT, 37 °C, and 65 °C) from top to bottom. The scale length for these images is 50 μm. The dotted yellow circles show salt deposits. Salt deposition was observed to increase with increasing KCl concentration.

3.3.2 FTIR SPECTRAL STUDY

FTIR was conducted on pure CA and CA-KCl fibers to determine the nature of the interactions between CA fibers and KCl. The absorption bands were identified [62] and reported in Table 1.

Table 1: Peak attribution of the characteristic peaks of pure CA [62]

Peak No.	Wavenumber (cm^{-1})	Corresponding Peak
1	1033	C-O-C of cellulose backbone
2	1217	C-O stretching of the acetyl group
3	1367	C-H bending vibration of CH3 in the acetyl group
4	1646	H-O-H bending of absorbed water
5	1738	C=O stretching of the acetyl group
6	2900-2950	C-H stretching of CH2 or CH
7	3400-3500	-OH stretching of unacetylated cellulose

FIGURE 7a shows four representative FT-IR plots for each type of fiber with offset %transmittance value on the y-axis for better comparison. All the peaks had nearly similar corresponding wavenumber except peak 2 attributed to C-O stretching of the acetyl group. FIGURE 7b shows a closer view of the overlap of all four types of fibers at peak 2. It revealed a deviation of around 10 cm^{-1}, which is consistent and notable enough [55] to indicate a potential chemical interaction between C-O bond in the acetyl group with the positively charged K^+ ions. FIGURE 7c provides additional information about this

interaction. While the shift was observed at all temperatures, the trend of the shift in wavenumber, however, changed with different drying temperatures, further indicating a chemical reaction.

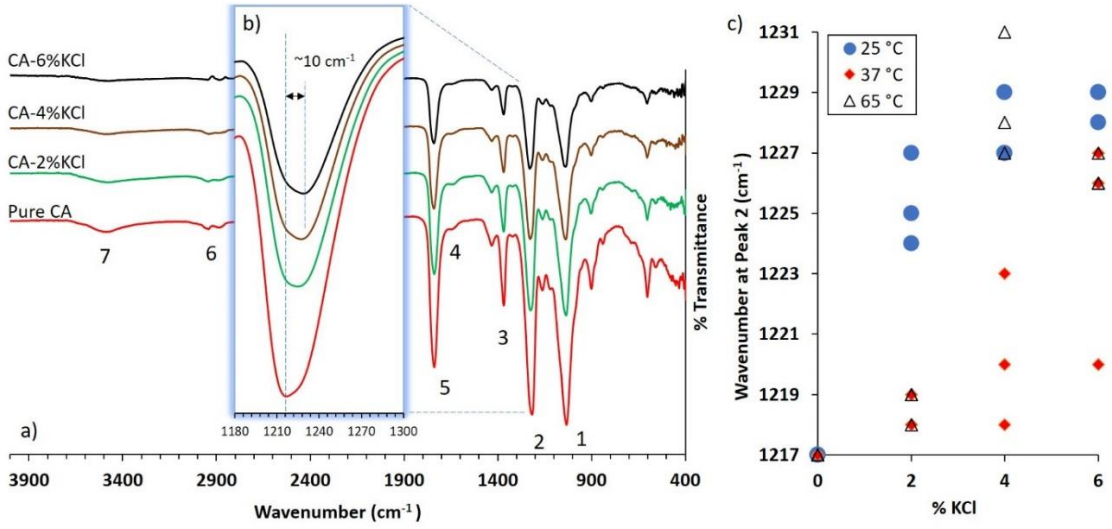

FIGURE 7: a) The FTIR-spectra of all four types of fibers air-dried at room temperature; b) Magnified view of the FTIR-spectra showing a 10 cm^{-1} deviation of wavenumber at peak 2 attributed to C-O stretching of the acetyl group; c) A scatter plot showing wavenumber at peak 2 for all types of fibers dried at different temperatures.

3.3.3 TENSILE RESPONSE OF CA VS. CA-KCL FIBERS

Multiple tensile tests were performed for pure CA (control sample), and each type of RT air-dried CA-KCl fibers to understand the effect of KCl on mechanical properties. The number of samples was 10, 9, 4, and 4 for pure CA, CA-2%KCl, CA-4%KCl, and CA-6%KCl, respectively. FIGURE 8 shows a stress-strain graph where each plot is a representative data of each type of fiber having stiffness closest to the average plot.

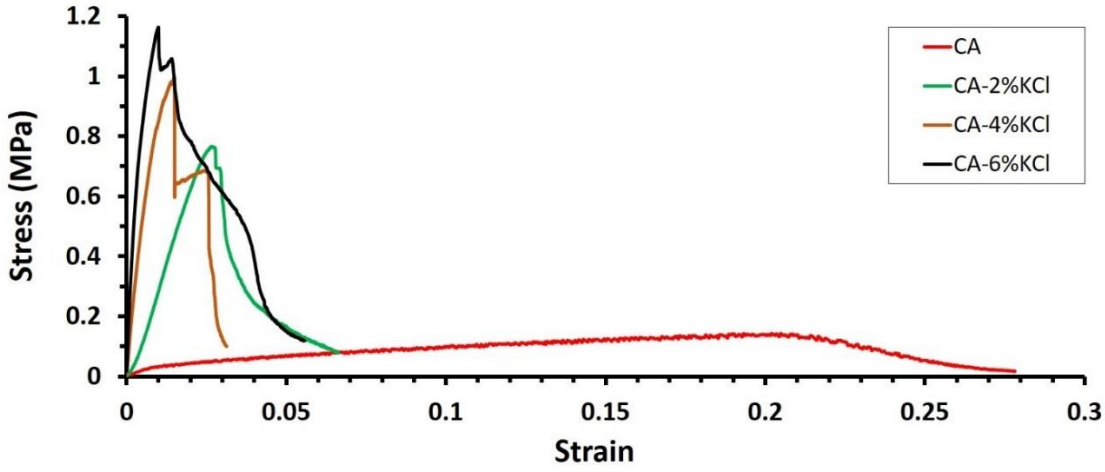

FIGURE 8: Representative stress-strain plot of each type of fibers

Mechanical properties such as elastic modulus, mechanical strength and percentage strain at failure has been calculated and represented in FIGURE 9.

For pure CA, the elastic modulus (up to 0.5 %strain) was 3.41 ± 0.67 MPa and tensile strength was 0.14 ± 0.02 MPa. For CA-2%KCl, the elastic modulus (up to 0.1 %strain) was 23.326 ± 8.72 MPa and tensile strength was 0.69 ± 0.20 MPa. For CA-4%KCl, the elastic modulus (up to 0.2 %strain) was 127.92 ± 44.56 MPa, and tensile strength was 1.10 ± 0.14 MPa. For CA-6%KCl, the elastic modulus (up to 0.2 %strain) was 176.14 ± 38.32 MPa, and tensile strength was 1.19 ± 0.13 MPa.

CA-2%KCl exhibited 6.8 times increase in the elastic modulus and 5 times increase in tensile strength. A significant difference (p value <0.05) in the mechanical property with respect to pure CA was observed. Subsequently, CA-4%KCl had a drastic increase in elastic modulus by 37.5 times and tensile strength by 8 times compared to pure CA. Lastly, CA-6%KCl fibers show a comparatively smaller rise in mechanical properties relative to CA-4%KCl with 51.7 times rise in elastic modulus and 8.62 times rise in tensile strength

compared to pure CA. A very insignificant difference in elastic modulus (p-value = 0.25) and tensile strength (p-value = 0.14) compared to CA-4%KCl was observed.

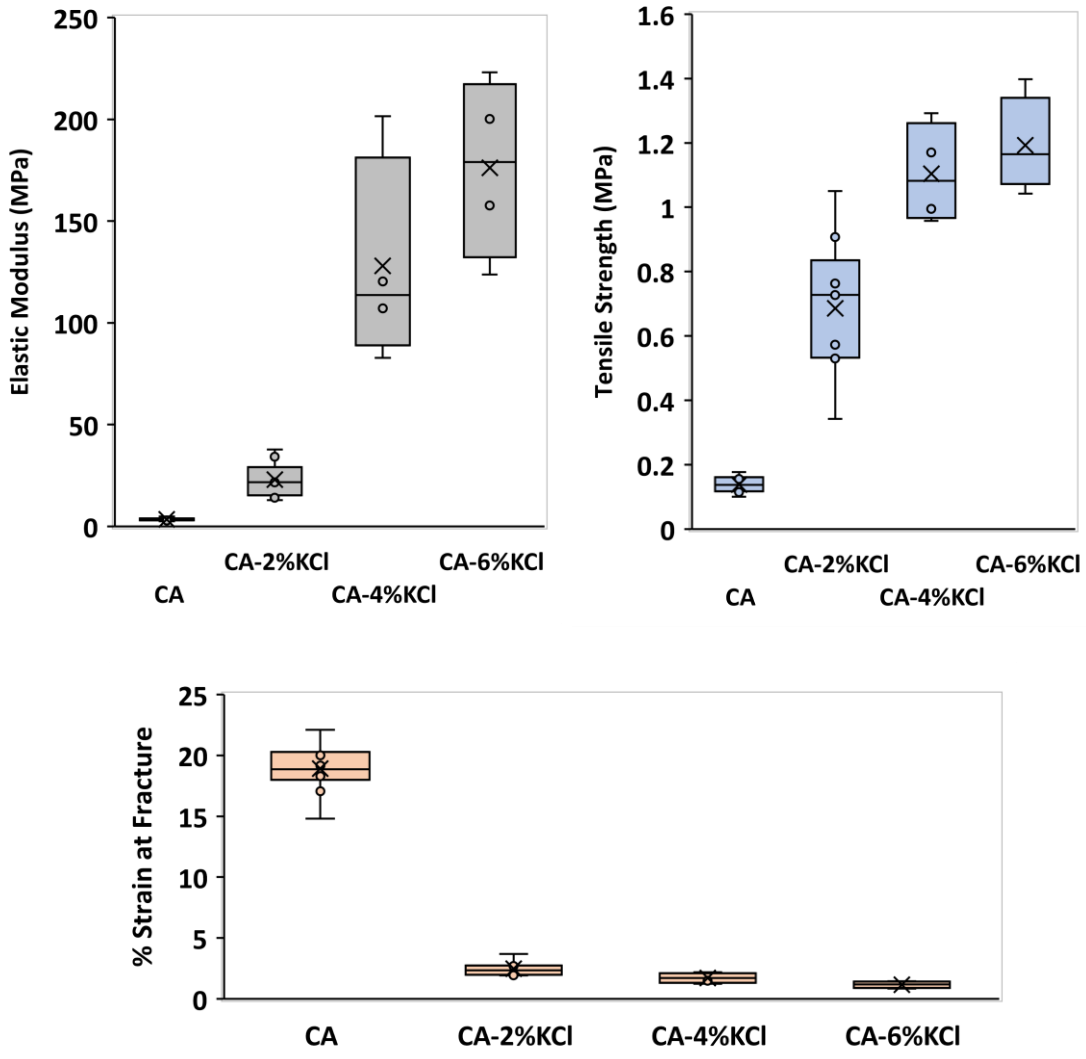

FIGURE 9: Mechanical properties represented as box plots: a) Elastic Modulus (in MPa) b) Tensile Strength (in MPa) c) Percentage strain at fracture

The percentage deviation of properties relative to their respective mean values was also calculated to understand the variation in results between types of samples. The mechanical

strength variation was highest in CA-2%KCl at ± 30% from its mean. For all others, the variation was between 10 to 17%.

3.3.4 DISCUSSION

The expected mechanism behind the increase in mechanical properties can be explained via a combination of two effects: salt deposition observed in SEM, and the chemical interaction of potassium ions and acetyl groups found via FTIR. For CA-2% KCl, the salt deposition is small, reflected in a minimum change in its relative weight (FIGURE 5) and in SEM images (FIGURE 6). Hence, impact from salt deposition on mechanical properties is expected to be minimal compared to the chemical interaction. The FTIR analysis indicated the potential chemical interaction between the C-O bond in the acetyl group with the positively charged K^+ ions (FIGURE 7). The drastic increase in stiffness and strength observed for CA-2%KCl (FIGURE 9) could be attributed primarily to chemical interactions. Also, the limited salt deposits were distributed randomly on the fiber mat (FIGURE 5), leading to a larger variation in tensile strengths.

In comparison, for CA-4% KCl and CA-6%KCl, salt deposits were more prominent and uniformly distributed observed via an increase of relative weight (FIGURE 5) and SEM data (FIGURE 6). For these samples, the increased salt concentration did not have a prominent further boost in strength. Together it indicates the higher impact of strength from chemical interaction as compared to increasing salt deposits on the stiffening of fibers. Secondary failure peaks were also observed for CA-KCl tensile response. The possibility of slippage of grips was ruled out due to the resurgence of stress after failure and in the consistency of the phenomenon across different samples. A closer look at the failure

locations (FIGURE 10) of the testing samples revealed two failure locations: the first one is on the outer surface, and the second one is on the inner surface. Thus, it is inferred that the mechanical behavior of the CA fibers in the inner folds is different than the outer. The inside folds have lower salt penetration leading to lower salt deposit and/or chemical interaction. Hence, the first failure peak is attributed to the failure of the stiffer outer zone, and the second failure is attributed to the failure of inner folds.

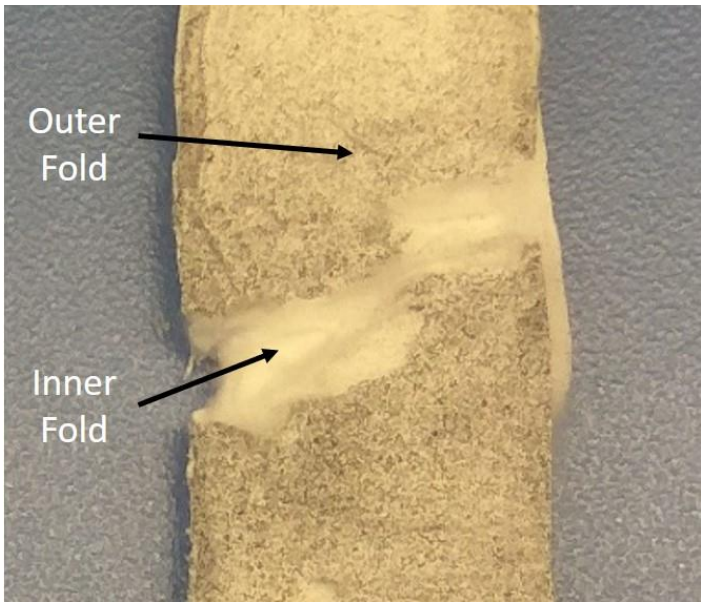

FIGURE 10: Magnified view of fracture zone of a CA-KCl fiber sample. The black dots are due to black sprays for better visibility

3.3.5 LIMITATION

The mechanical property of pure CA fiber, especially its tensile strength, seems to be on the lower end from values reported in other studies of electrospun CA fibers, as summarized in Table 2. It should be noted that the mechanical properties of the fiber mat

are very much dependent on the fiber diameter, the density of the network, and the degree of alignment. A model predicted 3.5 and 8.5 times increase in the modulus with the change in fiber alignment from isotropic to moderately aligned and highly aligned, respectively [63].

To investigate some of these aspects, fiber diameter analysis has been carried out on pure CA SEM image (FIGURE 4b) using DiameterJ, an extension to ImageJ/FIJI [64][65]. The result of the analysis is shown in FIGURE 11. The average cumulative diameter was found to be 0.827 ± 0.4057 μm. The fiber diameter reported in Table 2 varied from 200 nm to 13.3 μm, with a lower tensile stiffness value of 1.2 reported for diameters in the range of 0.2 to 1 μm.

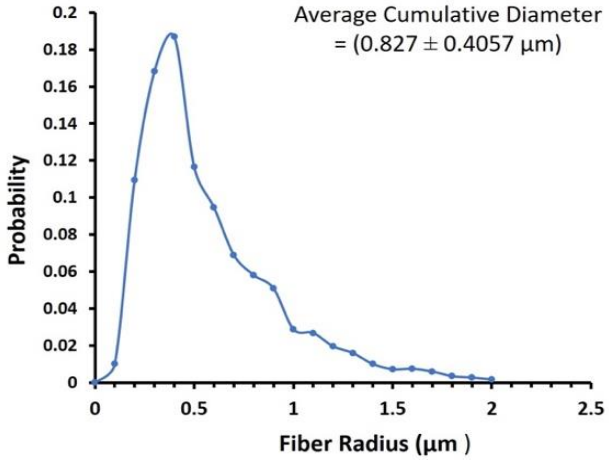

FIGURE 11: Fiber radius distribution of pure CA (FIGURE 4b) calculated using Image

*Please refer to the original source for this section: R. Sinha, S. Janaswamy, and A. Prasad, "Enhancing mechanical properties of Electrospun Cellulose Acetate Fiber Mat upon Potassium Chloride exposure," *Materialia*, vol.14, December 2020, Article 100881* 31

*Table 2: Different parameters used in electrospinning and tensile test samples of various modifications of CA fibers and the corresponding mechanical properties (*indicates data approximated from stress-strain plots; - indicates not reported)*

No.	Electrospinning parameters						Strain Rate	Fiber Diameter	Mechanical Property (pure CA)			Ref
	M_W	W_t %	Voltage	Distance	Flow Rate	Solvent			σ_T	E	ε_f	
	1000		(kV)	(cm)	(mL/h)		(mm/min)	(nm)	MPa	MPa	(%)	
1	29	-	25	15	4	Acetone:DMF:TFE (3:1:1)	10	200-1000	1.2*	1*	15*	[53]
2	50	-	26-28	15	0.07-0.14	Acetone:DMF (3:2)	-	515 ± 45	45*	100	44*	[31]
3	30	19	12	15	-	Acetone:DMF (3:2)	5	580 ± 200	-	247	-	[55]
4	50	15	27	15	0.13	Acetone:DMF (3:2)	2	300 ± 25	49	400	27*	[56]
5	30	-	20	10	6-18	TFA:acetic acid (7:3)	10	331 ± 118	2.16*	9*	4.5*	[54]
6	50	-	25	25	90	Ethyl Acetate	25	5×10^3	3.8	34.7	27	[57]
7	29	15	15	15	6	Acetone	0.2	$(13.3 \pm 3.5) \times 10^3$	-	7.3 ± 1.8	13	[63]
8	50	12	20	20	0.2	Acetone:DMF (2:1)	5	-	2-3	-	-	[66]
9	30	15	15	18	12	Acetone	2	827 ± 405.7	0.14 ± 0.4	3.41 ± 0.7	18.9 ± 1.3	This work

Additionally, large variations in electrospinning parameters also exist among studies. We used CA with molecular weight 30,000 g/mol, while studied reported values from 29,000 to 50,000. The concentration and type of solution is another factor influencing the outcome. The tensile modulus was reported to increase in the orders of 3.5 to 12.4 MPa as the concentration of CA in acetone rise from 10 to 17.5 % [63].

Finally, the different or unreported strain rate of the tensile tests also makes comparisons difficult. Taken together, these mismatches in fiber diameter, distribution, molecular weight, and solvent concentration are expected to be the underlying reasons for observed large property variation among sources. Moving forward, a way of validation and reporting fiber strength could be calculating the mechanical property of a single CA fiber, to compare against theoretical values. This approach will be taken in future studies such as the sonication-induced scission for fiber strength calculation [66].

*Please refer to the original source for this section: R. Sinha, S. Janaswamy, and A. Prasad, "Enhancing mechanical properties of Electrospun Cellulose Acetate Fiber Mat upon Potassium Chloride exposure," *Materialia*, vol.14, December 2020, Article 100881* 33

CHAPTER 4: **CONCLUSION AND FUTURE SCOPE**

4.1 SUMMARY AND CONCLUSION

Electrospun fibers CA fibers have been used widely in tissue engineering applications due to their optimum morphology and resorbability. However, pure CA fibers have inadequate mechanical properties, especially for bone tissue engineering. The proposed methodology of treating potassium chloride to cellulose acetate seems to be effective in enhancing the tensile mechanical properties along with its added benefits in bone cell proliferation, making it a promising biomaterial for bone tissue engineering. The mechanical properties such as tensile strength and elastic modulus can be increased 7 times from 0.2 MPa to 1.4 MPa and around 50 times from 4 MPa to 200 MPa respectively by increasing the KCl concentration. The presence of potassium ions yields added benefits desirable for bone tissue engineering. The study thus shows the implications of enhanced CA fiber in the presence of KCl. These results can have profound influence on bone tissue engineering applications. The proposed research thus also paves the way for future studies of enhanced CA-KCl 3D structures via lyophilization as cell-growth and bone-tissue microenvironment.

4.2 FUTURE WORK

4.2.1 LYOPHILIZATION

The two-dimensional shape of electrospun fiber can be a hindrance to its potential substitute for large bone defects. Studies have shown a significant deviation of results in cell activities from 2D to 3D matrix in terms of cell proliferation, differentiation, and mechanotransduction [68]. The pore size of a minimum 100 μm is required for osteogenesis and pores sizes greater than 350 μm for vascularization [69]. Lyophilization of cellulose acetate gel has been proven to control the porous structure to obtain the desired 3D morphology with micro and macro pores.

The compressive properties of the scaffold generated are equally crucial for efficient cell proliferation and should be able to withstand a physiological strain of 2500 με [70]. Hence, tuning the mechanical properties of the cellulose acetate scaffold obtained by lyophilization to achieve the desired strain environment using the proposed methodology of treating with potassium ion is one promising platform to develop 3D bone tissue microenvironment.

A preliminary experiment has been done but couldn't come up quantitative results due to time constraint. As a control sample, cellulose acetate was dissolved in acetic acid/ water solution (3:1, w/w) (total quantity: 80 mL) and kept overnight in a liquid nitrogen deep freezer overnight to solidify. After then, it was taken to a vacuum dryer to cool down at low pressure and -40 °C.

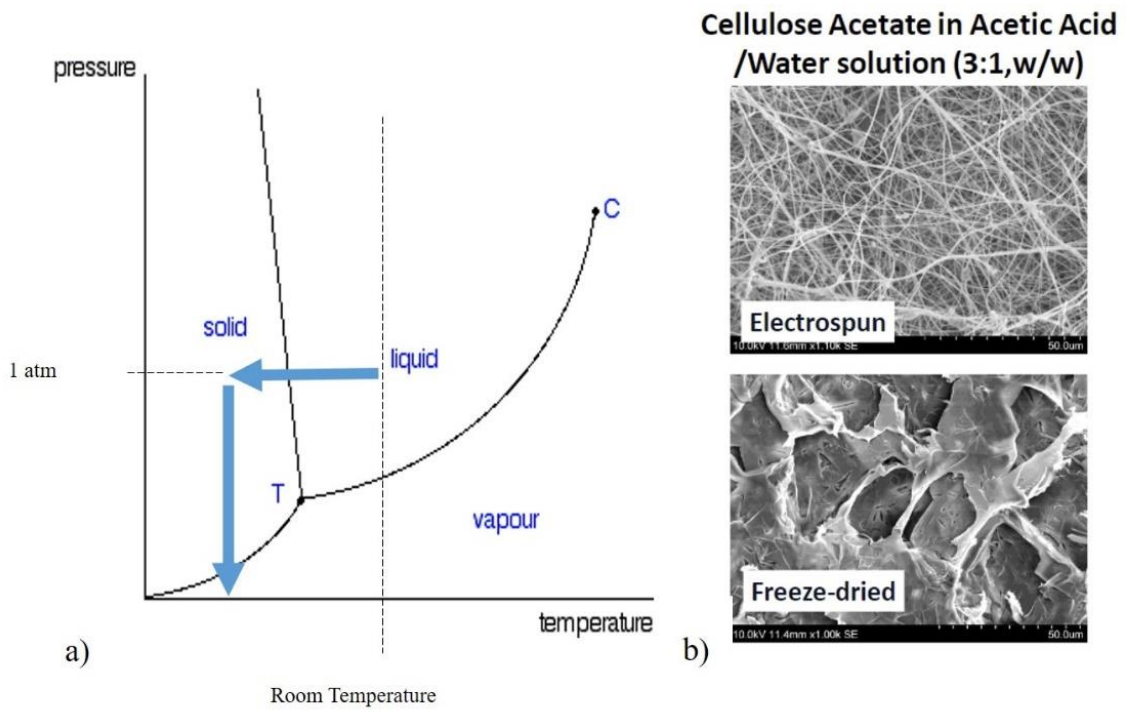

FIGURE 12: a) Pressure- Temperature diagram explaining the lyophilization process b) SEM image of Electrospun and Freeze-dried CA

FIGURE 13: Left to Right: 3D structure after lyophilization i) Pure CA ii) 0.5 wt% K-C, 2% KCl iii) 1.5 wt% K-C, 2% KCl iv) 1 wt% K-C, 2% KCl [K-C stands for k-carrageenan]

In other samples, k-carrageenan (a sulfated polysaccharide with strong tendency to gel formation on presence of K^+ ions) was also added at 0.5,1.0 and 1.5 wt% in the solution

and freeze-dried. It gave harder porous structure compared to the control sample which was fragile. The next step is to lyophilize cellulose acetate and KCl and check the mechanical properties by a compression test.

4.2.2 COMPUTATIONAL STUDY OF THE SCAFFOLD STRUCTURE

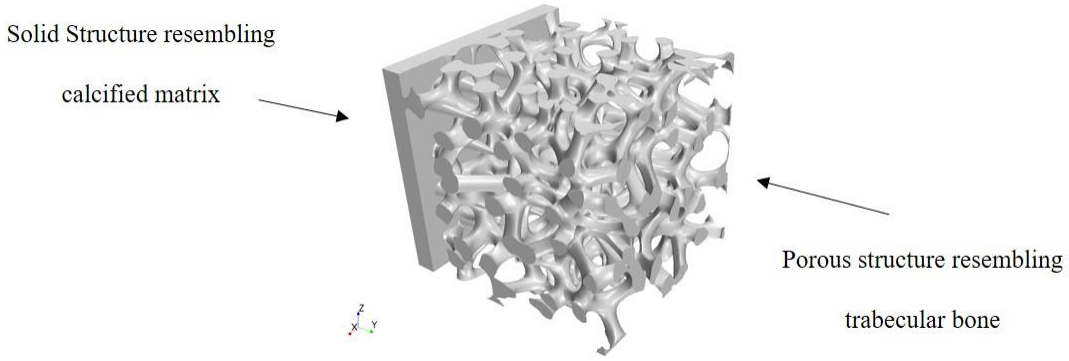

FIGURE 14: Generation of scaffold structure resembling trabecular bone

In order to predict the behavior of a scaffold structure with certain porosity under a perfusion media, a computational fluid mechanics study was performed. A 70% porous cubic (25 mm x 25 mm) structure was created performing Voronoi tessellation using *Rhino 3D*. As an output, stereolithographic file (.stl) was obtained that was imported to Star CCM+ 2019. Bone marrow flow parameters were referred from literature (viscosity = 0.4 Pa.s [modelled as Newtonian fluid], density= 0.9 g/cm^3= 900 kg/m^3 ,velocity of inlet = 100 µm/s, pressure of outlet = 0 Pa) [71] and assumed to be the perfusion flow parameter. Two different kind of boundary condition were applied (FIGURE 15), and the wall shear stress exerted was compared. It was found that the distribution of wall shear stress in both the boundary condition were similar and suitable to generate an osteogenic response in multipotent stromal cells and pre-osteoblastic cells (FIGURE 16).

Boundary Condition 1: Orientation of the bone scaffold to place calcified cartilage **on top** while placing on the base platform of the bioreactor setup

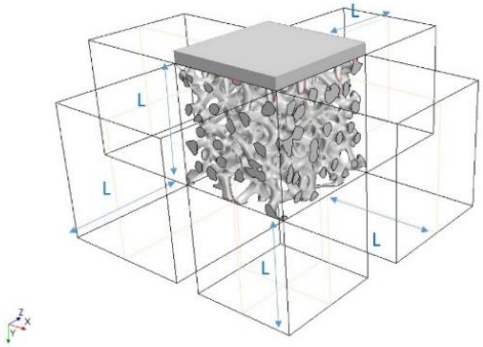

Fluid region (length L) outside the scaffold

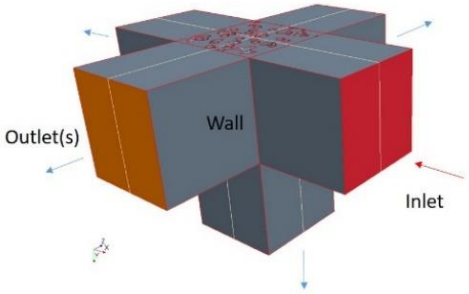

Boolean Subtract to get Fluid region (input for CFD analysis)

Boundary Condition 2: Orientation of the bone scaffold to place calcified cartilage **on the face opposite to the flow** while placing on the base platform of the bioreactor setup

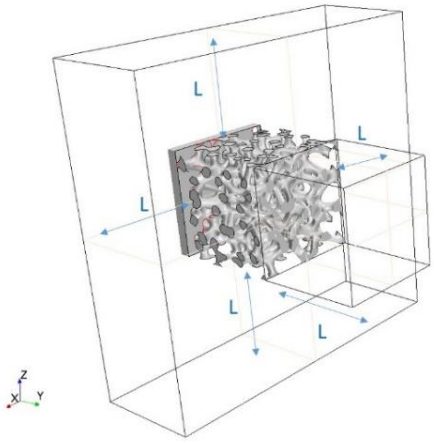

Fluid region (length L) outside the scaffold

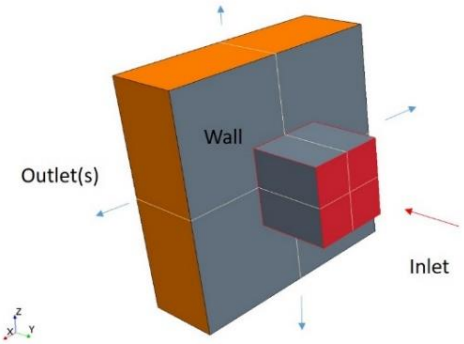

Boolean Subtract to get Fluid region (input for CFD analysis)

FIGURE 15: Different boundary conditions for fluid mechanics study of flow of bone marrow through the bone structure

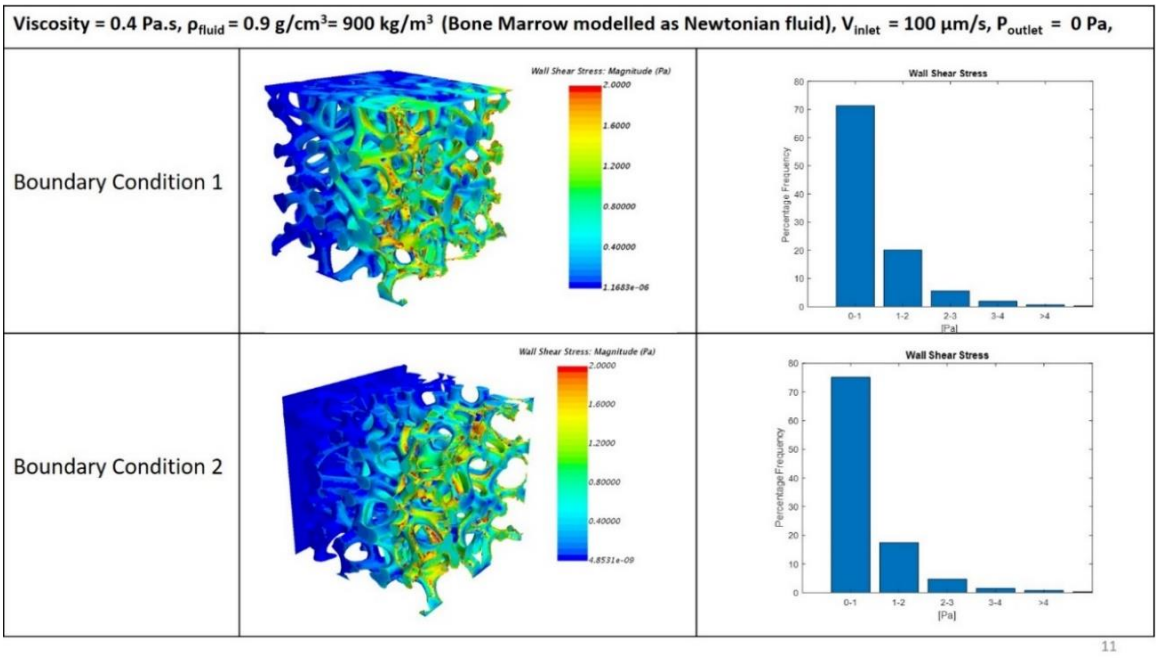

FIGURE 16: Wall shear stress under two different boundary conditions

In order to mimic an external load and study its effect on the strain environment of the bone, a computational solid mechanics simulation was performed. However, this required conversion of stl file (surface mesh) into a volume mesh.

The software ANSYS ICEM CFD was used to perform the conversion to a 4-noded tetrahedral mesh (FIGURE 17). The output file was saved as cfx5 file format due to the convenience of its listing of node and element information.

The volume mesh was then imported to ANSYS APDL and the material property of isolated collagen fiber was assumed. This works can be a foundation for the studying the scaffold whose material property will be obtained experimentally.

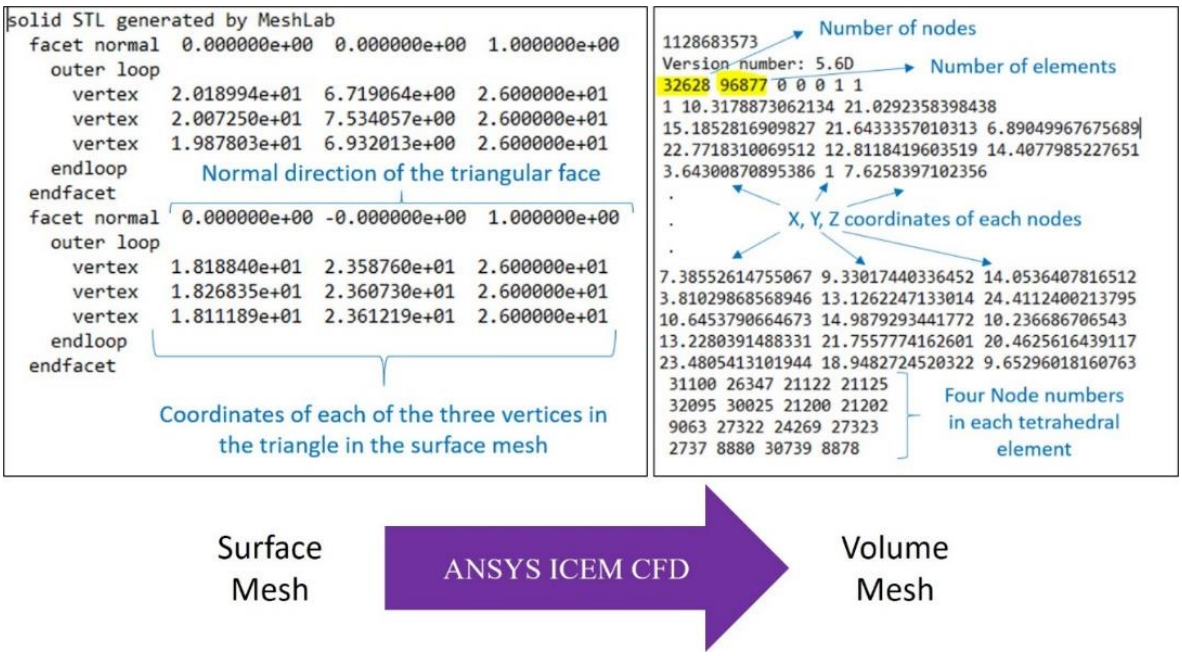

FIGURE 17: Conversion of stl file to cfx file.

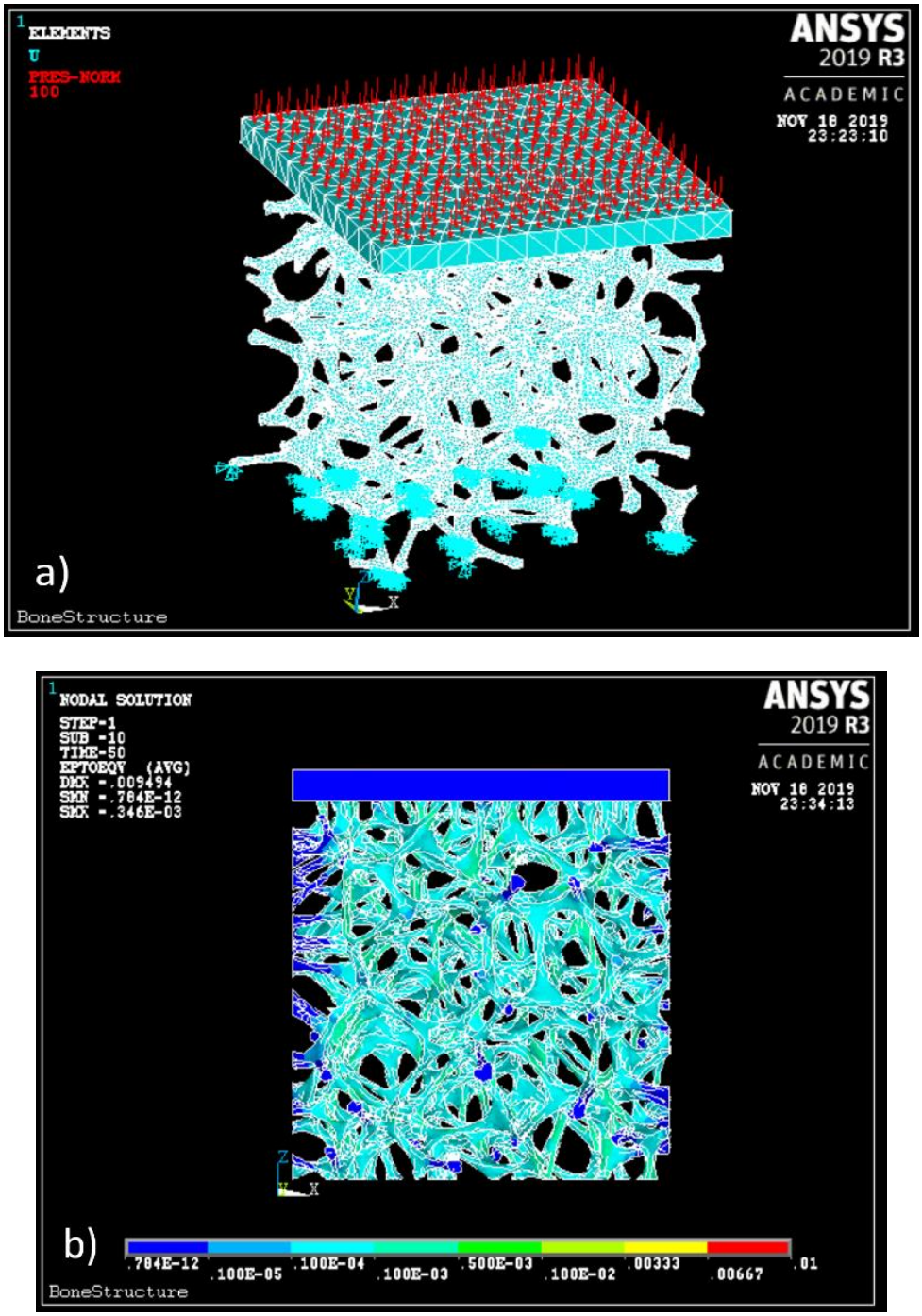

FIGURE 18: Strain environment of the scaffold structure under an arbitrary pressure of 100 MPa

4.2.3 APPENDIX:

ANSYS APDL commands to perform the computational solid mechanics:

```
/Title,BoneStructure
/FILNAME,3DSolid
/UNITS,BIN          !length-m, mass-kg, stress-Pa


/PREP7              ! preprocessor
ET,1,SOLID285       ! 4-noded tetrahedral element (for scaffold)
KEYOPT, 1, 16, 1    ! Enable steady state analysis
ET,2,SOLID187       ! 10-noded tetrahedral element (for contact plate)
KEYOPT, 1, 16, 1    ! Enable steady state analysis
ET,3,CONTA174       ! 3D 8-node surface-to-surface Contact element
ET,4,TARGE170       ! 3D Target element


MP,EX,1,152e6       ! Initial Young's Modulus(Bone)= Einfinity+E1+E2
MP,NUXY,1,0.3       ! poisson's ratio
MP,EX,2,10e9        ! Plate Young's Modulus = 10GPa
MP,NUXY,2,0.2       ! poisson's ratio
MP,MU,3,0.2         ! friction coefficient of contact surface


!small strain viscoelasticity
TB,PRONY,1,,2,SHEAR           !define viscosity parameters (shear)
TBDATA,1,0.0855,7,0.1053,102  ! m1,t1,m2,t2; m= prony series parameters
TB,PRONY,1,,2,BULK            !define viscosity parameters (bulk)
TBDATA,1,0.0855,7,0.1053,102  ! m1,t1,m2,t2; m= prony series parameters
```

```
TYPE,1
MAT,1
! node number and coordinates imported from volume mesh
N,    1     ,     1     ,     10.31788731 ,     21.02923584
N,    2     ,     15.18528169 ,     21.6433357  ,     6.890499677
N,    3     ,     22.77183101 ,     12.81184196 ,     14.40779852
N,    4     ,     3.643008709 ,     1     ,     7.62583971
.
.
.
N,    32625 ,     3.810298686 ,     13.12622471 ,     24.41124002
N,    32626 ,     10.64537907 ,     14.98792934 ,     10.23668671
N,    32627 ,     13.22803915 ,     21.75577742 ,     20.46256164
N,    32628 ,     23.48054131 ,     18.94827245 ,     9.652960182

! nodes numbers in each element
E,    31100 ,     26347 ,     21122 ,     21125
E,    32095 ,     30025 ,     21200 ,     21202
E,    9063  ,     27322 ,     24269 ,     27323
E,    2737  ,     8880  ,     30739 ,     8878
.
.
.
E,    9935  ,     9934  ,     69    ,     21363
E,    30995 ,     19906 ,     864   ,     800
E,    1100  ,     21074 ,     4     ,     22601
```

```
! Contact Surface
NSEL,s,loc,z,26          ! selection of nodes at z=26 mm
TYPE,4                   ! assigning element no. 4
MAT,3                    ! assigning material no. 3
ESURF ! Generates elements overlaid on the free faces of selected nodes.
ALLSEL,ALL
SMRTSIZE,1
VMESH,1                  ! Volume mesh command
ASEL,s,,,1   ! area of plate in contact with top most face of scaffold
NSLA,s,1     ! selection of all nodes in previous selected area

BLOCK,1,26,1,26,26,28    ! Plate geometry
TYPE,2                   ! assigning element no. 2
MAT,2                    ! assigning material no. 2
TYPE,3       ! assigning element no. 3
MAT,3
ESURF
ALLSEL,ALL

finish
/solution

ANTYPE,TRANS,new            ! Transient Analysis
NLGEOM,ON                   ! Turn on Large Deflection Effects

! displacement constraint
NSEL,s,loc,z,0,1
D,all,all,0
NSEL,all
```

```
!pressure
NSEL,s,loc,z,28
SF,all,PRES,100 ! in MPa
NSEL,all


TIME,50           ! Analysis till 50 seconds
OUTRES,all,-10    ! Number of result outputs = 10
DELTIM,1,1,5      ! first delta time, min delta time, max delta time


SOLVE
finish
!nsel,s,loc,z,20,25
!remove '!'sign to check result at user defined node location
!esln,s,1


!esel,s,type,,3
!remove '!'sign to check elements at contact surface
```

CHAPTER 5: **REFERENCES**

[1] S. A. Goldstein, “The mechanical properties of trabecular bone: Dependence on anatomic location and function,” *J. Biomech.*, vol. 20, no. 11–12, pp. 1055–1061, 1987.

[2] R. Oftadeh, M. Perez-Viloria, J. C. Villa-Camacho, A. Vaziri, and A. Nazarian, “Biomechanics and Mechanobiology of Trabecular Bone: A Review,” *J. Biomech. Eng.*, vol. 137, no. 1, 2015.

[3] M. Pawlikowski, K. Skalski, J. Bańczerowski, A. Makuch, and K. Jankowski, “Stress–strain characteristic of human trabecular bone based on depth sensing indentation measurements,” *Biocybern. Biomed. Eng.*, vol. 37, no. 2, pp. 272–280, 2017.

[4] E. F. Morgan, H. H. Bayraktar, and T. M. Keaveny, “Trabecular bone modulus-density relationships depend on anatomic site,” *J. Biomech.*, vol. 36, no. 7, pp. 897–904, 2003.

[5] E. F. Morgan, G. U. Unnikrisnan, and A. I. Hussein, “Bone Mechanical Properties in Healthy and Diseased States,” *Annu. Rev. Biomed. Eng.*, vol. 20, no. 1, pp. 119–143, 2018.

[6] “DoITPoMS - TLP Library Structure of bone and implant materials.” [Online]. Available: https://www.doitpoms.ac.uk/tlplib/bones/printall.php. [Accessed: 09-Dec-2018].

[7] M. J. Olszta *et al.*, “Bone structure and formation : A new perspective,” vol. 58, pp. 77–116, 2007.

[8] Bilezikian JP, Raisz LG, Rodan GA, *Principles of Bone Biology*. 1996.

[9] I. D. Xynos, M. V. J. Hukkanen, J. J. Batten, L. D. Buttery, L. L. Hench, and J. M. Polak, “Bioglass 45S5 Stimulates Osteoblast Turnover and Enhances Bone Formation In Vitro : Implications and Applications for Bone Tissue Engineering,” pp. 321–329, 2000.

[10] L. Roseti *et al.*, “Scaffolds for Bone Tissue Engineering: State of the art and new perspectives,” *Mater. Sci. Eng. C*, vol. 78, pp. 1246–1262, 2017.

[11] X. B. Yang *et al.*, “Human Osteoprogenitor Growth and Differentiation on Synthetic Biodegradable Structures After Surface Modification,” vol. 29, no. 6, pp. 523–531, 2001.

[12] R. Agarwal and A. J. García, “Biomaterial strategies for engineering implants for enhanced osseointegration and bone repair,” *Adv. Drug Deliv. Rev.*, 2015.

[13] S. Torgbo and P. Sukyai, “Bacterial cellulose-based scaffold materials for bone tissue engineering,” *Appl. Mater. Today*, vol. 11, pp. 34–49, 2018.

[14] S. Sofia, M. B. Mccarthy, G. Gronowicz, D. L. Kaplan, and S. E. T. Al, “Functionalized silk-based biomaterials for bone formation,” 2000.

[15] L. Meinel *et al.*, “Engineering bone-like tissue in vitro using human bone marrow stem cells and silk scaffolds,” 2004.

[16] J. Perez-Rigueiro, C. Viney, J. Llorca, and M. Elices, “Silkworm Silk as an Engineering Material,” *J. Appl. Polym. Sci.*, vol. 70, pp. 2439–2447, 1998.

[17] R. Nazarov, H. Jin, and D. L. Kaplan, “Porous 3-D Scaffolds from Regenerated Silk Fibroin,” *Biomacromolecules*, vol. 5, pp. 718–726, 2004.

[18] D. Klemm, B. Heublein, H. Fink, and A. Bohn, “Polymer Science Cellulose :

Fascinating Biopolymer and Sustainable Raw Material Angewandte," pp. 3358–3393, 2005.

[19] M. Pang, Y. Huang, F. Meng, Y. Zhuang, H. Liu, and M. Du, "Application of bacterial cellulose in skin and bone tissue engineering," *Eur. Polym. J.*, no. July, p. 109365, 2019.

[20] F. Granero-molto *et al.*, "Role of mesenchymal stem cells in regenerative medicine : application to bone and cartilage repair Role of mesenchymal stem cells in regenerative medicine : application to bone and cartilage repair," vol. 2598, no. August, 2017.

[21] Q. Shi *et al.*, "The osteogenesis of bacterial cellulose scaffold loaded with bone morphogenetic protein-2," *Biomaterials*, vol. 33, no. 28, pp. 6644–6649, 2012.

[22] Y. J. Lee *et al.*, "The effect of thickness of resorbable bacterial cellulose membrane on guided bone regeneration," *Materials (Basel).*, vol. 10, no. 3, 2017.

[23] Y. Kwan *et al.*, "Fabrication of bacterial cellulose-collagen composite sca ff olds and their osteogenic e ff ect on human mesenchymal stem cells," *Carbohydr. Polym.*, vol. 219, no. February, pp. 210–218, 2019.

[24] R. J. Hickey and A. E. Pelling, "Cellulose biomaterials for tissue engineering," *Front. Bioeng. Biotechnol.*, vol. 7, no. MAR, 2019.

[25] V. Karageorgiou and D. K. Ã, "Porosity of 3D biomaterial scaffolds and osteogenesis," vol. 26, pp. 5474–5491, 2005.

[26] J. D. Currey, "Tensile yield in compact bone is determined by strain , post-yield behaviour by mineral content," vol. 37, pp. 549–556, 2004.

[27] J. Y. Rho, R. B. Ashman, and C. H. Turner, "Young's modulus of trabecular and

cortical bone material: Ultrasonic and microtensile measurements," *J. Biomech.*, vol. 26, no. 2, pp. 111–119, 1993.

[28] K. Tashiro and M. Kobayashi, "Theoretical evaluation of three-dimensional elastic constants of native and regenerated celluloses: role of hydrogen bonds," *Polymer (Guildf).*, vol. 32, no. 8, pp. 1516–1526, 1991.

[29] S. Yamanaka *et al.*, "The structure and mechanical properties of sheets prepared from bacterial cellulose," *J. Mater. Sci.*, vol. 24, no. 9, pp. 3141–3145, 1989.

[30] X. Feng *et al.*, "Characterization of Bacterial Cellulose by Gluconacetobacter hansenii CGMCC 3917," *J. Food Sci.*, vol. 80, no. 10, pp. E2217–E2227, 2015.

[31] A. Salama, A. Mohamed, N. M. Aboamera, T. Osman, and A. Khattab, "Characterization and mechanical properties of cellulose acetate/carbon nanotube composite nanofibers," *Adv. Polym. Technol.*, vol. 37, no. 7, pp. 2446–2451, 2018.

[32] N. M. Aboamera, A. Mohamed, A. Salama, T. A. Osman, and A. Khattab, "Characterization and mechanical properties of electrospun cellulose acetate/graphene oxide composite nanofibers," *Mech. Adv. Mater. Struct.*, vol. 6494, no. December, pp. 1–5, 2017.

[33] Q. Xu, C. Chen, K. Rosswurm, T. Yao, and S. Janaswamy, "A facile route to prepare cellulose-based films," *Carbohydr. Polym.*, vol. 149, pp. 274–281, 2016.

[34] L. M. Ilharco and R. Brito De Barros, "Aggregation of pseudoisocyanine iodide in cellulose acetate films: Structural characterization by FTIR," *Langmuir*, vol. 16, no. 24, pp. 9331–9337, 2000.

[35] J. D. Boerckel, C. V. Gemmiti, D. E. Mason, Y. M. Kolambkar, B. D. Porter, and R. E. Guldberg, *Physical Stress as a Factor in Tissue Growth and Remodeling*, no.

3. Elsevier Inc., 2019.

[36] E. Ruoslahti and M. D. Pierschbacher, “New perspectives in cell adhesion: RGD and integrins,” *Science (80-.).*, vol. 238, no. 4826, pp. 491–497, 1987.

[37] S. Vukicevic, F. P. Luyten, H. K. Kleinman, and A. H. Reddi, “Differentiation of canalicular cell processes in bone cells by basement membrane matrix components: Regulation by discrete domains of laminin,” *Cell*, vol. 63, no. 2, pp. 437–445, 1990.

[38] A. Rezania and K. E. Healy, “Biomimetic peptide surfaces that regulate adhesion, spreading, cytoskeletal organization, and mineralization of the matrix deposited by osteoblast-like cells,” *Biotechnol. Prog.*, vol. 15, no. 1, pp. 19–32, 1999.

[39] B. A. Dalton, C. D. McFarland, P. A. Underwood, and J. G. Steele, “Role of the heparin binding domain of fibronectin in attachment and spreading of human bone-derived cells,” *J. Cell Sci.*, vol. 108, no. 5, pp. 2083–2092, 1995.

[40] R. Pértile, S. Moreira, F. Andrade, L. Domingues, and M. Gama, “Bacterial cellulose modified using recombinant proteins to improve neuronal and mesenchymal cell adhesion,” *Biotechnol. Prog.*, vol. 28, no. 2, pp. 526–532, 2012.

[41] A. R. Tsiapla *et al.*, “Biomimetic and biodegradable cellulose acetate scaffolds loaded with dexamethasone for bone implants,” *Beilstein J. Nanotechnol.*, vol. 9, no. 1, pp. 1986–1994, 2018.

[42] Y. Chen, T. Xi, Y. Zheng, L. Zhou, and Y. Wan, “In Vitro Structural Changes of Nano-Bacterial Cellulose immersed in Phosphate Buffer Solution,” vol. 10, pp. 55–66, 2011.

[43] P. Gouma, R. Xue, C. P. Goldbeck, P. Perrotta, and C. Balázsi, “Nano-hydroxyapatite - Cellulose acetate composites for growing of bone cells,” *Mater.*

Sci. Eng. C, vol. 32, no. 3, pp. 607–612, 2012.

[44] D. Atila, D. Keskin, and A. Tezcaner, "Crosslinked pullulan/cellulose acetate fibrous scaffolds for bone tissue engineering," *Mater. Sci. Eng. C*, vol. 69, pp. 1103–1115, 2016.

[45] L. Wang *et al.*, "Electrospun nanofiber-reinforced three-dimensional chitosan matrices: Architectural, mechanical and biological properties," *J. Colloid Interface Sci.*, vol. 565, pp. 416–425, 2020.

[46] S. Mayer-Wagner *et al.*, "Membrane-based cultures generate scaffold-free neocartilage in vitro: Influence of growth factors," *Tissue Eng. - Part A*, vol. 16, no. 2, pp. 513–521, 2010.

[47] D. Atila, D. Keskin, and A. Tezcaner, "Cellulose acetate based 3-dimensional electrospun scaffolds for skin tissue engineering applications," *Carbohydr. Polym.*, vol. 133, pp. 251–261, 2015.

[48] S. Farzamfar *et al.*, "Neural tissue regeneration by a gabapentin-loaded cellulose acetate/gelatin wet-electrospun scaffold," *Cellulose*, vol. 25, no. 2, pp. 1229–1238, 2018.

[49] A. P. Kishan and E. M. Cosgriff-Hernandez, "Recent advancements in electrospinning design for tissue engineering applications: A review," *J. Biomed. Mater. Res. - Part A*, vol. 105, no. 10, pp. 2892–2905, 2017.

[50] A. Haider, S. Haider, and I. K. Kang, "A comprehensive review summarizing the effect of electrospinning parameters and potential applications of nanofibers in biomedical and biotechnology," *Arab. J. Chem.*, vol. 11, no. 8, pp. 1165–1188, 2018.

[51] S. Majumder, M. A. Matin, A. Sharif, and M. T. Arafat, “Understanding solubility, spinnability and electrospinning behaviour of cellulose acetate using different solvent systems,” *Bull. Mater. Sci.*, vol. 42, no. 4, pp. 1–9, 2019.

[52] H. Liu and Y. Lo Hsieh, “Ultrafine fibrous cellulose membranes from electrospinning of cellulose acetate,” *J. Polym. Sci. Part B Polym. Phys.*, vol. 40, no. 18, pp. 2119–2129, 2002.

[53] Z. Ma, M. Kotaki, and S. Ramakrishna, “Electrospun cellulose nanofiber as affinity membrane,” *J. Memb. Sci.*, vol. 265, no. 1–2, pp. 115–123, 2005.

[54] D. N. Phan, H. Lee, B. Huang, Y. Mukai, and I. S. Kim, “Fabrication of electrospun chitosan/cellulose nanofibers having adsorption property with enhanced mechanical property,” *Cellulose*, vol. 26, no. 3, pp. 1781–1793, 2019.

[55] M. Gopiraman, K. Fujimori, K. Zeeshan, B. S. Kim, and I. S. Kim, “Structural and mechanical properties of cellulose acetate/graphene hybrid nanofibers: Spectroscopic investigations,” *Express Polym. Lett.*, vol. 7, no. 6, pp. 554–563, 2013.

[56] N. M. Aboamera, A. Mohamed, A. Salama, and A. Khattab, “Characterization and mechanical properties of electrospun cellulose acetate/graphene oxide composite nanofibers,” *Mech. Adv. Mater. Struct.*, vol. 26, no. 9, pp. 765–769, 2019.

[57] K. I. Lukanina, T. E. Grigoriev, S. V. Krasheninnikov, V. G. Mamagulashvilli, R. A. Kamyshinsky, and S. N. Chvalun, “Multi-hierarchical tissue-engineering ECM-like scaffolds based on cellulose acetate with collagen and chitosan fillers,” *Carbohydr. Polym.*, vol. 191, no. December 2017, pp. 119–126, 2018.

[58] H. Ishikawa and S. Tadano, “Mechanical and optical characterization of cellulose

acetate," *Exp. Mech.*, vol. 28, no. 3, pp. 221–225, 1988.

[59] C. Y. Zheng, S. J. Li, X. J. Tao, Y. L. Hao, R. Yang, and L. Zhang, "Calcium phosphate coating of Ti-Nb-Zr-Sn titanium alloy," *Mater. Sci. Eng. C*, vol. 27, no. 4, pp. 824–831, 2007.

[60] S. N. Nayab, F. H. Jones, and I. Olsen, "Human alveolar bone cell adhesion and growth on ion-implanted titanium," *J. Biomed. Mater. Res. - Part A*, vol. 69, no. 4, pp. 651–657, 2004.

[61] E. Goldstein, J; Newbury, Dale E.; Echlin, Patrick; Joy, David C.; Romig Jr., Alton D. ; Lyman, Charles E.; Fiori, Charles ; Lifshin, *Scanning Electron Microscopy and X-Ray Microanalysis: A Text for Biologists, Materials Scientists, and Geologists*, 2nd ed. New York and London: Springer US, 1992.

[62] P. Fei, L. Liao, B. Cheng, and J. Song, "Quantitative analysis of cellulose acetate with a high degree of substitution by FTIR and its application," *Anal. Methods*, vol. 9, no. 43, pp. 6194–6201, 2017.

[63] T. Stylianopoulos *et al.*, "Tensile mechanical properties and hydraulic permeabilities of electrospun cellulose acetate fiber meshes," *J. Biomed. Mater. Res. Part B Appl. Biomater.*, vol. 100B, no. 8, pp. 2222–2230, 2012.

[64] J. Schindelin *et al.*, "Fiji: an open-source platform for biological-image analysis," *Nat. Methods 2012 97*, vol. 9, no. 7, pp. 676–682, Jun. 2012.

[65] N. A. Hotaling, K. Bharti, H. Kriel, and C. G. Simon, "DiameterJ: A validated open source nanofiber diameter measurement tool," *Biomaterials*, vol. 61, pp. 327–338, 2015.

[66] J. Avõ, S. N. Fernandes, and M. H. Godinho, "Revealing the hierarchical mechanical

strength of single cellulose acetate electrospun filaments through ultrasonic breakage," *Macromol. Rapid Commun.*, vol. 36, no. 12, pp. 1166–1170, 2015.

[67] R. Sinha, S. Janaswamy, and A. Prasad, "Enhancing mechanical properties of Electrospun Cellulose Acetate Fiber Mat upon Potassium Chloride exposure," *Materialia*, vol. 14, no. May, p. 100881, 2020.

[68] K. Duval *et al.*, "Modeling physiological events in 2D vs. 3D cell culture," *Physiology*, vol. 32, no. 4, pp. 266–277, 2017.

[69] O. Petrauskaite, G. Juodzbalys, P. Viskelis, and J. Liesiene, "Control of the porous structure of cellulose-based tissue engineering scaffolds by means of lyophilization," *Cellul. Chem. Technol.*, vol. 50, no. 1, pp. 23–30, 2016.

[70] Y. Yan *et al.*, "Mechanical Strain Regulates Osteoblast Proliferation through Integrin-Mediated ERK Activation," vol. 7, no. 4, pp. 1–14, 2012.

[71] E. Birmingham, G. L. Niebur, L. M. McNamara, and P. E. McHugh, "An Experimental and Computational Investigation of Bone Formation in Mechanically Loaded Trabecular Bone Explants," *Ann. Biomed. Eng.*, vol. 44, no. 4, pp. 1191–1203, 2016.